nature immunology

ARTICLES

https://doi.org/10.1038/s41590-021-01027-8

Check for updates

Transposon-triggered innate immune response confers cancer resistance to the blind mole rat

Yang Zhao[1], Ena Oreskovic[1], Quanwei Zhang[2], Quan Lu[1], Abbey Gilman[1], Yifei S. Lin[1], Junyue He[1], Zhizhong Zheng[1], J. Yuyang Lu[1], Jina Lee[1], Zhonghe Ke[1], Julia Ablaeva[1], Matthew J. Sweet[3], Steve Horvath[4], Zhengdong Zhang[2], Eviatar Nevo[5], Andrei Seluanov[1,6] ✉ and Vera Gorbunova[1,6] ✉

Blind mole rats (BMRs) are small rodents, characterized by an exceptionally long lifespan (>21 years) and resistance to both spontaneous and induced tumorigenesis. Here we report that cancer resistance in the BMR is mediated by retrotransposable elements (RTEs). Cells and tissues of BMRs express very low levels of DNA methyltransferase 1. Following cell hyperplasia, the BMR genome DNA loses methylation, resulting in the activation of RTEs. Upregulated RTEs form cytoplasmic RNA–DNA hybrids, which activate the cGAS–STING pathway to induce cell death. Although this mechanism is enhanced in the BMR, we show that it functions in mice and humans. We propose that RTEs were co-opted to serve as tumor suppressors that monitor cell proliferation and are activated in premalignant cells to trigger cell death via activation of the innate immune response. Activation of RTEs is a double-edged sword, serving as a tumor suppressor but contributing to aging in late life via the induction of sterile inflammation.

Animals that are naturally cancer resistant provide powerful models to uncover novel anticancer mechanisms that may be applicable to humans[1]. Blind mole rats (BMRs), *Spalax*, are small, long-lived subterranean rodents found in the Middle East, with a maximum lifespan which exceeds 21 years[2–4]. The BMR displays strong resistance to both spontaneous and induced tumorigenesis[2,3]. In a previous study, we demonstrated that BMRs prevent cancer through a mechanism termed concerted cell death (CCD), which is triggered by the secretion of interferon (IFN)-β after 7–20 population doublings to prevent hyperplasia[2]. However, the mechanism by which CCD is induced has remained unknown.

Transposable elements (TEs) are mobile repetitive sequences and major components of eukaryotic genomes[5]. As examples in mammals, TEs make up 45 (ref. [6]) and 37.5% (ref. [7,8]) of the human and mouse genomes, respectively. The process of retrotransposition could cause mutations by interrupting a gene sequence and/or leave a cleaved genome unrepaired[9–11]. Retrotransposable elements (RTEs) are epigenetically silenced by DNA methylation[12,13]. DNA methyltransferase 1 (DNMT1) is responsible for the maintenance of DNA methylation. DNMT1 recognizes hemi-methylated CpG sites and methylates the unmethylated DNA[14,15]. Multiple other mechanisms have evolved to silence RTEs (reviewed in[5]). Activation of LINE-1 (L1) resulting from a loss of epigenetic silencing during aging and senescence has been shown to trigger sterile inflammation and cell death due to the formation of cytoplasmic RTE copies that activate the innate immune response[16–18]. Therefore, active retrotransposition has been associated with aging and diseases related to aging.

The potential role of RTEs in driving tumorigenesis has been investigated. Large-scale sequencing efforts identified multiple de novo somatic insertions in human tumors[19–21]. Insertions into tumor-suppressor genes, such as *APC* in colon cancer[22] and *PTEN* in endometrial carcinoma[20], have been found and linked to development of the cancer. However, the majority of de novo insertions in cancers seem to be passenger events[23]. On the contrary, emerging evidence suggests that RTEs serve as tumor suppressors. Treatment of cancer cells with demethylating agents or LSD1 ablation, which removes RTE silencing, triggers cell death via the activation of endogenous retroviruses (ERVs) and the double-stranded RNA (dsRNA)-sensing pathway[24,25]. These studies suggest that forced reactivation of RTEs can have an antitumor effect. It was recently shown that L1s serve as tumor suppressors by triggering genomic instability in myeloid leukemia[26].

Here we investigated the mechanisms of tumor resistance in a naturally tumor-resistant rodent, the BMR. We discovered that the BMR has naturally low DNMT1 activity. This results in the loss of methylation on RTEs following cell hyperplasia, leading to the formation of cytoplasmic RTE RNA/DNA and cell death via the activation of the cyclic GMP–AMP synthase (cGAS)–stimulator of IFN genes (STING)–IFN pathway. Furthermore, we show that this mechanism functions in mice and in human xenografts. Analysis of the Cancer Cell Line Encyclopedia (CCLE) database revealed that L1 activation in human cancer cells correlates positively with the number of mutations in the cGAG–STING–IFN pathway, providing further evidence that L1s act as tumor suppressors in humans. Our study reveals a beneficial function of RTEs as tumor suppressors.

Results

The type I IFN pathway is activated in BMR cells undergoing CCD. During hyperproliferation primary BMR cells trigger CCD via an unknown mechanism[2]. To understand the mechanisms triggering CCD, we compared the transcriptomes of BMR fibroblasts undergoing CCD with those of low-passage growing cells.

[1]Department of Biology, University of Rochester, Rochester, NY, USA. [2]Albert Einstein College of Medicine, Bronx, NY, USA. [3]Institute for Molecular Bioscience, The University of Queensland, Brisbane, Queensland, Australia. [4]University of California, Los Angeles, CA, USA. [5]University of Haifa, Haifa, Israel. [6]Department of Medicine, University of Rochester Medical Center, Rochester, NY, USA. ✉e-mail: andrei.seluanov@rochester.edu; vera.gorbunova@rochester.edu

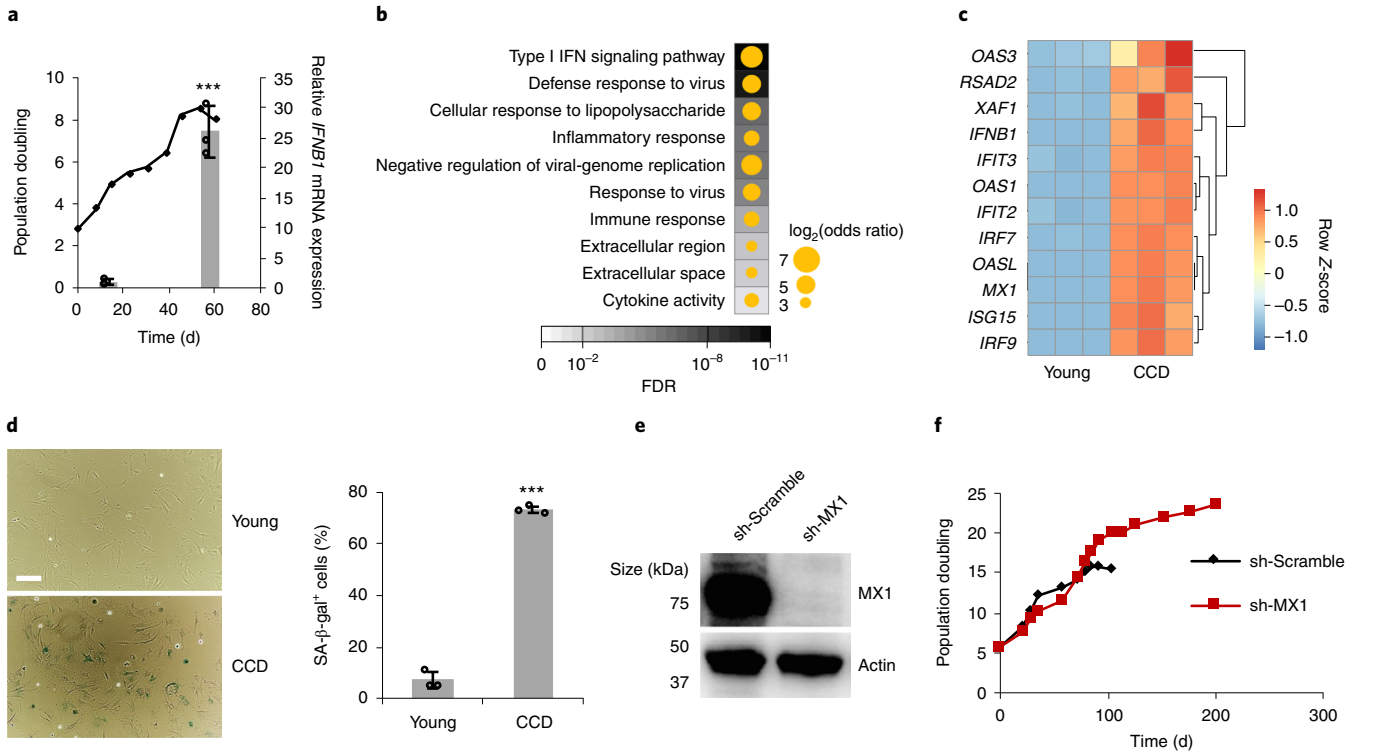

Fig. 1 | Activation of the IFN response in overproliferating BMR cells triggers CCD. a, Upregulation of *IFNB1* gene expression (bars) before CCD. **b**, Top ten Gene ontology terms of the most upregulated genes (fold change > 10 and false discovery rate (FDR) < 0.05) in a comparison between young and CCD cells. The background color represents the FDR and the dot size represents the odds ratio. **c**, Heatmap showing the relative expression of all 12 genes from the type I IFN pathway that were upregulated in CCD cells compared with young cells. **d**, Images (left) and quantification (right) of SA-β-gal staining of young and CCD cells. Scale bar, 10 μM. **e**, Western blot showing knockdown of the IFN-induced gene *MX1* by shRNA (sh-MX1). The experiment was repeated three times independently with similar results. **f**, Growth curve showing that the knockdown of *MX1* rescued CCD. **a**,**d**, Data are the mean ± s.d.; ***$P < 0.001$, unpaired two-sided Student's *t*-test.

The messenger RNA levels of the *IFNB1* gene, which encodes IFN-β, increased dramatically before the onset of CCD (Fig. 1a). Whole-transcriptome RNA sequencing (RNA-seq) confirmed that type I IFN, inflammation and immune response pathways are enriched within the genes that are most upregulated (Fig. 1b). A total of 12 genes from the type I IFN pathway were exclusively upregulated (Fig. 1c). The cells entered cell-cycle arrest immediately before (~2 d) the onset of CCD and displayed characteristics of cellular senescence, as determined by senescence-associated β-galactosidase (SA-β-gal) staining (Fig. 1d) and the expression of senescence markers and senescence-associated secretory phenotype genes (SASP; Extended Data Fig. 1a,b). One of the most upregulated genes, *MX1*, is an IFN-inducible gene responsible for inducing cell death[27]. Knockdown of *MX1* rescued CCD (Fig. 1e,f). Therefore, CCD is triggered by the type I IFN response.

In BMR tissues, multiple immunity-related pathways are expressed at lower levels compared with mice (Extended Data Fig. 1c). These pathways include *cGAS*, *STING*, multiple interferon-regulatory-factor genes from the IFN pathway and *Nfkb1* from the canonical NF-κB pathway (Extended Data Fig. 1d). In contrast, the *Irf2* gene and the noncanonical NF-κB pathway gene *Nfkb2*, both of which negatively regulate the activation of IFN[28–30], had higher expression levels in the BMR tissues than in mice (Extended Data Fig. 1d). Interestingly, many of the genes that are expressed at lower levels in the BMR were upregulated in BMR CCD cells—including the *Nfkb1* gene and IFN pathway genes—whereas the *Nfkb2* gene, which is expressed at higher levels, was downregulated during CCD (Fig. 1c and Extended Data Fig. 1e), showing an opposite trend in CCD when compared with normal tissues. This result suggests that IFN-related genes are repressed in normal BMR tissues to prevent accidental activation of CCD.

RTEs are activated in BMR cells before the onset of CCD. Type I IFN is a major component of the innate immune response. Typically, the type I IFN pathway is activated during viral infection. It can also be triggered by nuclear DNA leaking into the cytoplasm as a result of chromatin degradation or retrotransposon activity[16,17,31]. We therefore examined whether RTEs are activated during CCD. The expression levels of RTEs were analyzed using RNA-seq comparing low-passage cells to cells entering CCD. Many RTEs were upregulated before the onset of CCD (Fig. 2a), including ERVs, SINEs and LINEs (Fig. 2b). As SINEs and LINEs are highly repetitive elements, consensus sequences of SINE B1 and B2, and L1 were detected by quantitative PCR with reverse transcription (RT–qPCR) to confirm upregulation (Fig. 2c). The PCR primers were designed to detect the consensus sequences of the major RTEs; therefore, the results reflect the expression of multiple RTE groups. When tracking the expression of RTEs with cellular proliferation, we noticed that their expression levels gradually increased with the onset of CCD (Fig. 2d). We also detected increased expression of L1 open reading frame 1 (ORF1) protein, indicating that active, autonomous L1 elements, which provide reverse transcriptase for other RTEs, were also derepressed (Fig. 2e). To further confirm that the increase in SINE and LINE transcripts was not caused by read-through transcription, we performed 5′ rapid amplification of complementary DNA ends (RACE) and found that most of the transcriptional start sites of SINE B1 are very close to its consensus Pol III promoter start site and

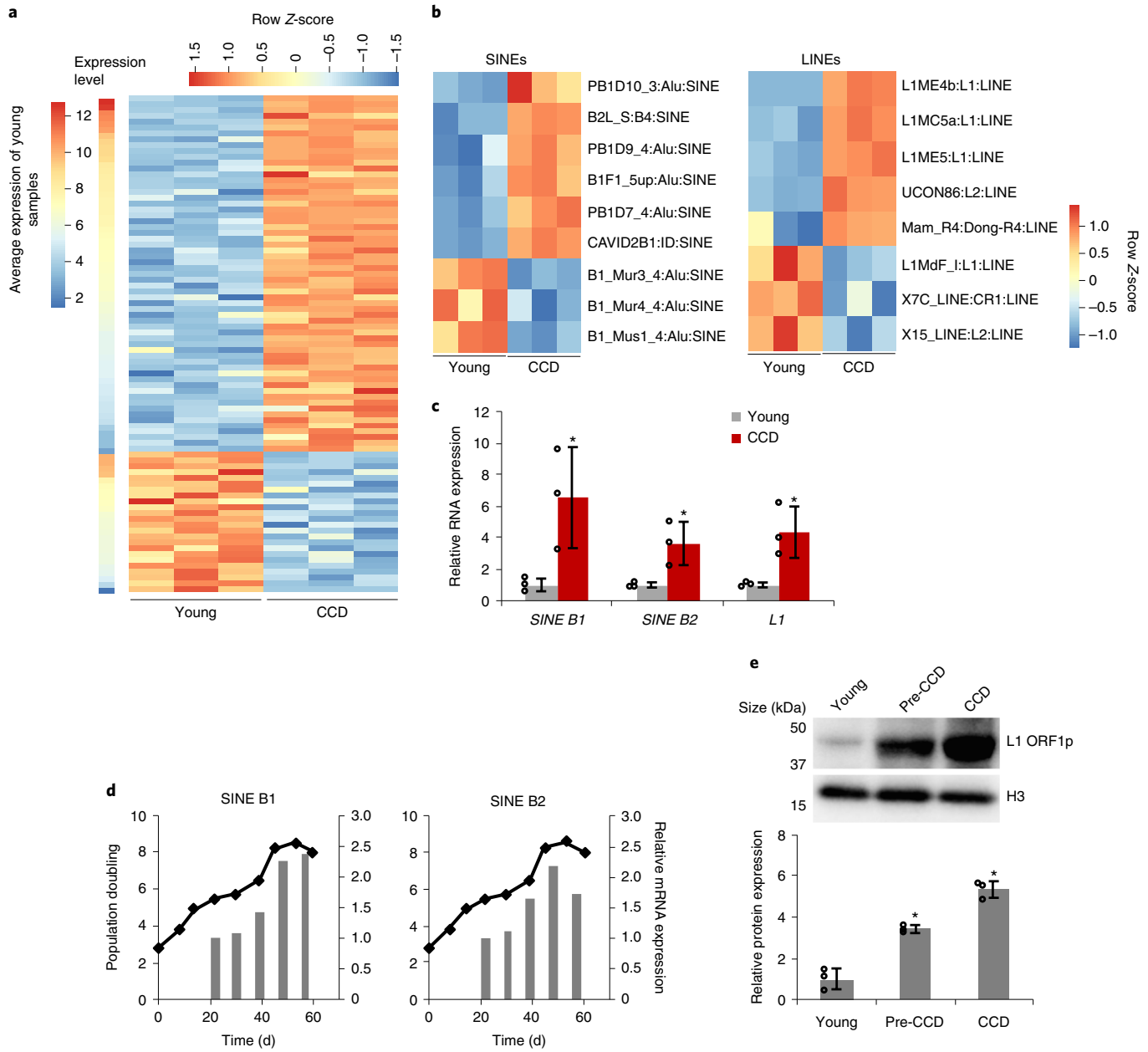

Fig. 2 | Retrotransposons are activated in overproliferating BMR cells to trigger IFN and CCD due to naturally weak DNMT1. a, Heatmap showing TEs ($P < 0.01$; fold change > 1.5) that were differentially expressed between young and CCD cells. The TEs were sorted based on the average basal expression level in young cells for upregulated and downregulated TEs, separately. To determine statistically significant differences, FDR-adjusted *P* values were used. **b**, Heatmaps showing SINE (left) and LINE (right) retrotransposons that were differentially expressed between young and CCD cells. For SINE elements, the number after the name of the subfamily (for example, '3' in 'PB1D10_3:Alu:SINE') indicates the number of CpGs in this element, by which instances of B1 subfamilies were further divided into subgroups. To distinguish different instances of the same type of TE, a sequential number was manually added to the instances of the same type of TE. **c**, Increased expression of *SINE B1*, *SINE B2* and *L1* in BMR CCD cells. RT–qPCR was performed using primers targeting the consensus sequence of rodent *SINE B1*, *SINE B2* and *L1* (*L1MdaI*) *ORF1*. **d**, Accumulation of *SINE B1* and *SINE B2* (bars), determined using RT–qPCR, with proliferation of BMR cells (lines). **e**, Western blot detecting L1 ORF1 (top) showing accumulation of L1 with proliferation of BMR cells (bottom). Histone H3 was used as a loading control. **c**,**e**, Data are the mean ± s.d. of three independent experiments. $^*P < 0.05$, unpaired two-sided Student's *t*-test.

those of L1 are within the 5′ untranslated region (UTR; Extended Data Fig. 2).

Topical treatment with tumorigenic 7,12-dimethylbenz(a) anthracene (DMBA) and 12-O-tetradecanoylphorbol-13-acetate (TPA), which fails to induce skin cancer in the BMR, also resulted in the general activation of RTEs and IFN expression in the treated BMR skin (Extended Data Fig. 3), suggesting the IFN response observed in cell culture is involved in cancer resistance of BMRs in vivo.

Activation of RTEs in BMR is due to low expression of DNMT1. Given that induction of RTEs may lead to genomic instability, RTEs are epigenetically silenced by DNA methylation[12,13]. The spontaneous activation of RTEs in overproliferating BMR cells indicated a

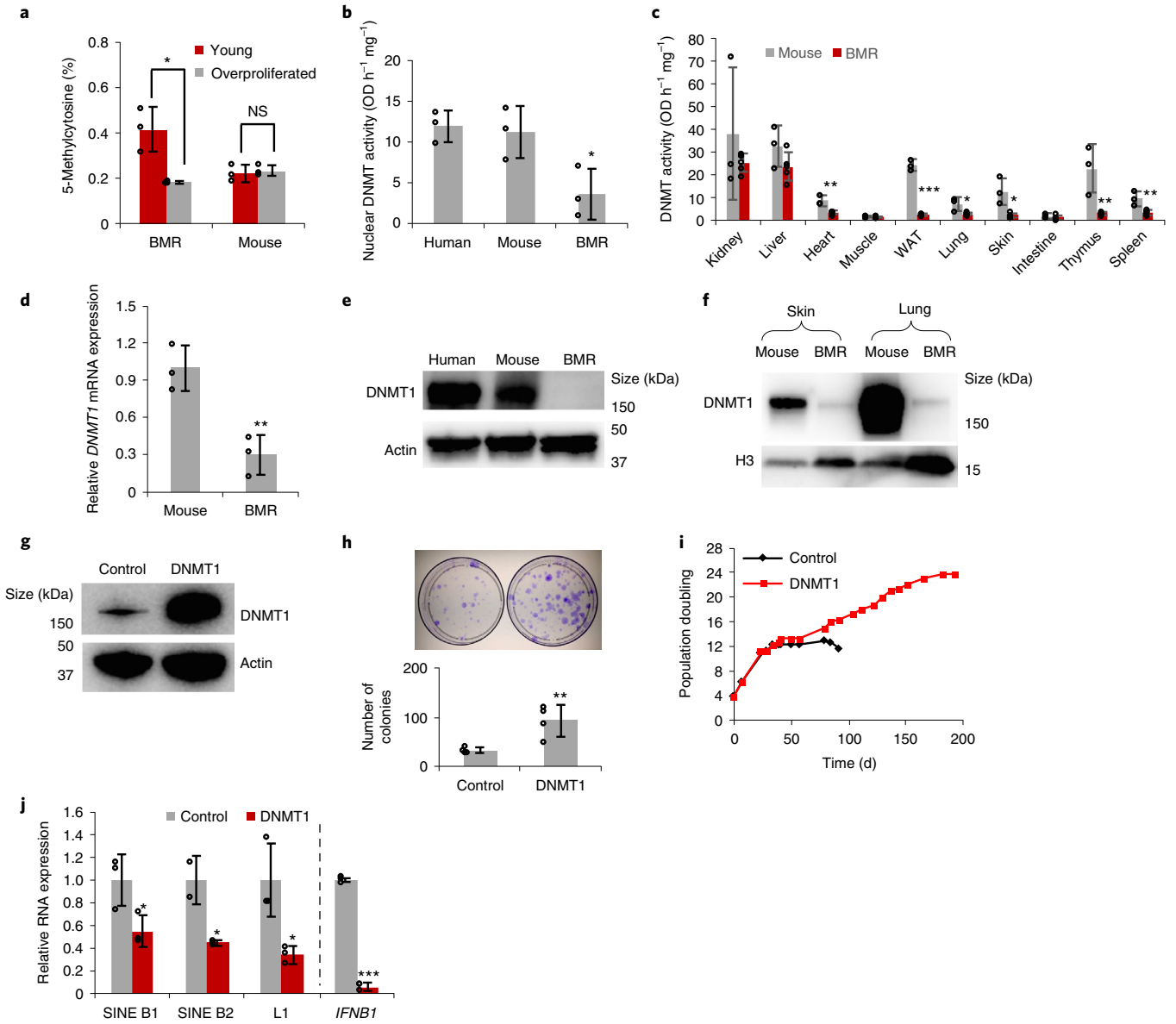

Fig. 3 | Naturally weak DNMT1 in BMR is responsible for RTE induction and CCD. a, Loss of global DNA methylation with the proliferation of BMR cells. **b**, Levels of DNMT activity in the nuclear extract of human, mouse and BMR fibroblasts. **c**, The BMR generally has weaker DNMT activity in its tissues. The DNMT activity in the nuclear extract was determined for different tissues from mice and BMRs. The experiments were performed using tissues from five BMRs and three mice. WAT, white adipose tissue. **d**,**e**, Analysis using RT–qPCR (**d**) and western blotting (**e**) showing that BMR cells have naturally low DNMT1 levels. **a**,**b**,**d**,**e**, The experiments were performed using three independent cell lines from each species. **f**, Western blot showing naturally lower levels of DNMT1 protein in the skin and lung tissues of BMRs compared with mice. **g**, Western blot showing overexpression of human DNMT1 in BMR cells. **h**, Overexpression of DNMT1 enhanced BMR cell growth. A clonogenic assay was performed using crystal violet staining (top). The quantification (bottom) is based on four independent experiments. **i**, Overexpression of DNMT1 rescued CCD. **f**,**g**,**i**, The experiments were repeated three times independently with similar results. **j**, Overexpression of DNMT1 repressed the expression of the retrotransposons SINE B1, SINE B2 and L1 as well as IFNB1, determined by RT–qPCR from three independent cell lines. **a**–**d**,**h**,**j**, Data are the mean ± s.d. NS, not significant; $^{*}P < 0.05$; $^{**}P < 0.01$, $^{***}P < 0.001$; unpaired two-sided Student's *t*-test.

loss of epigenetic silencing. The global DNA methylation levels in cells undergoing CCD indeed dropped sharply relative to young cells, whereas the methylation levels remained unchanged in proliferating mouse fibroblasts at the same population doubling (Fig. 3a). Using HorvathMammalMethylChip40, which profiles about 37,000 highly conserved CpG probes across mammals, we compared the general methylation profiles of the BMR and mouse in an unbiased manner. An unsupervised hierarchical clustering analysis revealed that BMR cells with a high population doubling are globally distinct from cells with a low population doubling, suggesting a dramatic epigenetic change with the proliferation of BMR cells. In contrast, no clustering effect was detected in mouse cells (Extended Data Fig. 4a). Methylated-DNA immunoprecipitation (MeDIP) was performed to ensure the coverage of TEs, and confirmed that the majority of RTEs—especially SINEs and LINEs—were hypo-methylated in dying BMR cells (Extended Data Fig. 4b), corresponding to the upregulation of RTEs shown by RNA-seq (Fig. 2a,b). In particular, the master sequence of SINE B1, the PB1D9 family[32], was upregulated

and demethylated in CCD cells (Fig. 2a,b and Extended Data Fig. 4b). In mammals, DNMT1 is responsible for the maintenance of DNA methylation[14,15]. We compared the DNMT activity of the nuclear extracts of human, mouse and BMR fibroblasts. Whereas the human and mouse cells had comparable nuclear DNMT activities, the BMR nuclear extract had much weaker activity (Fig. 3b). Nuclear extracts from multiple tissues of the BMR also had weaker DNMT activities than mouse tissues (Fig. 3c). Furthermore, the mRNA and protein levels of DNMT1 in the BMR cells were significantly lower than mouse and human cells (Fig. 3d,e). Low levels of DNMT1 expression were also observed in both skin and lung tissues (Fig. 3f). A multiple alignment of DNMT1 protein was performed to rule out the possibility of an inter-species influence on antibody recognition. The sequence of the antibody immunogen is highly conserved across humans, mice and BMRs, and humans and BMRs have identical sequences (Extended Data Fig. 4d). Furthermore, endogenous DNMT1 from BMR cells transfected with the SV40 Large T (LT) antigen, which is known to elevate DNMT1 expression[33], was easily detected (Extended Data Fig. 4e). An RNA-seq comparison of BMRs and mice showed lower expression of BMR *DNMT1* mRNA in different tissues (Extended Data Fig. 4c). These results suggest that the BMR has naturally low expression of DNMT1.

To investigate whether the naturally weak DNMT1 is responsible for the proliferation-induced activation of RTEs, we stably overexpressed human DNMT1 in BMR fibroblasts using the piggyBac (pPB) transposon system (Fig. 3g and Extended Data Fig. 4f). Ectopic expression of DNMT1 not only enhanced BMR cell growth, as determined by a clonogenic assay (Fig. 3h), but also rescued CCD (Fig. 3i). As expected, DNMT1-rescued cells had restored global DNA methylation levels (Extended Data Fig. 4g) and repressed expression of SINE B1, SINE B2, L1, *IFNB1* gene and senescence factors (Fig. 3j and Extended Data Fig. 4h). Collectively, these results suggest that the naturally weak DNMT1 of the BMR is responsible for the activated RTE-mediated IFN response and CCD.

As CCD involves a transient senescence-like state, we tested whether senescence was associated with DNA damage. Shortly before entering CCD, cells showed elevated γH2AX foci and DNA fragmentation, measured using a comet assay (Extended Data Fig. 5a,b). In agreement with this, a typical DNA damage response was observed, as determined by increased phosphorylation of Chk2 (Thr68) and p53 (Ser15) before CCD (Extended Data Fig. 5c). Notably, DNMT1-rescued cells displayed reduced DNA damage (Extended Data Fig. 5d). To determine whether the DNA damage is a cause or consequence of the IFN response, we treated young growing cells with either medium enriched with BMR IFN or conditioned medium from dying BMR cells. Both treatments induced DNA damage in young cells (Extended Data Fig. 5e), suggesting that the observed DNA damage is at least partly a consequence of the IFN response.

RTEs form cytoplasmic RNA–DNA hybrids and induce cGAS–STING. We next investigated the mechanism by which the RTEs induce an IFN response. Activated RTEs induce the IFN response by triggering an accumulation of cytoplasmic RTE DNA copies, which activate cytoplasmic DNA sensors[16,17]. The RTE-derived cytoplasmic nucleic acids can be of different types—including double-stranded and single-stranded DNA, dsRNA and RNA–DNA hybrids—depending on the types of RTEs that are activated[5]. As BMR cells contain many activated retrotransposons (SINEs and LINEs) before CCD, we detected the presence of both dsRNA and RNA–DNA hybrids. Although no differences in the levels of dsRNA were observed (Extended Data Fig. 6a), RNA–DNA hybrids were dramatically increased in CCD cells, as determined by immunofluorescence (Fig. 4a,b). Cells that were treated with RNase H (which specifically degrades RNA–DNA hybrids) and cells incubated with secondary antibody only lost cytoplasmic staining signals (Extended Data Fig. 6b), thereby confirming that the observed signals specifically represent RNA–DNA hybrids. Strikingly, the RNA–DNA hybrid signal was significantly reduced in DNMT1-rescued cells, suggesting the causal role of weak DNMT1 for RTE-derived cytoplasmic RNA–DNA hybrids (Fig. 4a,b).

RNA–DNA hybrids have been shown to activate the cGAS–STING pathway[34]. Considering that both IFN and SASP were induced in dying BMR cells, we hypothesized that the cGAS–STING–NF-κB pathway is activated to trigger CCD. Homo-dimers of STING (hallmark of STING activation) and phosphorylated NF-κB p65 Ser536 were indeed observed in CCD cells, and were both abrogated in DNMT1-rescued cells (Fig. 4c). To further confirm that the cGAS–STING pathway is responsible for CCD induction, we knocked down *cGAS* and *STING* using short hairpin RNA (shRNA; Extended Data Fig. 6e,f); both the cGAS and *STING* knockdowns rescued CCD and inhibited the expression of *IFNB1* and SASP genes (Fig. 4d,e). As expected, knockdown of dsRNA-sensing genes did not rescue CCD (Extended Data Fig. 6g).

It was previously shown[16,17] that the treatment of human and mouse cells with nucleoside reverse-transcriptase inhibitors (NRTIs) prevents the accumulation of cytoplasmic RTE DNA. Although NRTIs were developed as anti-human immunodeficiency virus (HIV) drugs, they also inhibit L1 reverse transcriptase[35]. We treated BMR cells with two NRTIs: abacavir and zidovudine. As expected, both treatments reduced the cytoplasmic RNA–DNA hybrids (Extended Data Fig. 6c). More importantly, NRTI treatment rescued CCD (Fig. 4f), repressed the expression of *IFNB1* and SASP genes (Fig. 4g), and reduced DNA damage (Extended Data Fig. 6d). Furthermore, the NRTIs also inhibited the cGAS–STING pathway by abrogating the STING dimer (Fig. 4h). To determine the specific DNA elements that bind and trigger cGAS, we performed an immunoprecipitation of cGAS. We purified the cGAS-bound DNA and SINE B1 and L1 enrichment was quantified using qPCR. The B1 and L1 sequences were enriched by nine- and 19-fold, respectively, in the CCD cells relative to young cells (Fig. 4i). Furthermore, we directly detected B1 and L1 cDNA in the cytoplasm of CCD cells

Fig. 4 | The cGAS–STING pathway is activated in overproliferating BMR cells by RNA–DNA hybrids and is required to induce the IFN response and CCD. a, Immunofluorescence images of cytoplasmic RNA–DNA hybrids stained with antibody to S9.6 comparing young, CCD and DNMT1-overexpressing (CCD + DNMT1) BMR cells. Scale bar, 5 μM. **b**, Levels of cytoplasmic RNA–DNA hybrids. Approximately 100 cells from each group were quantified for intensity. **c**, Activation of the cGAS–STING–NF-κB pathway in BMR CCD cells. Western blot showing STING dimer and phosphorylated NF-κB p65 (Ser536), which were repressed by overexpression of DNMT1. Histone H3 was used as a loading control. **d**, Knockdown of *cGAS* (sh-cGAS) or *STING* (sh-STING) rescued CCD of BMR cells. **e**, Knockdown of *cGAS* or *STING* in BMR cells repressed the expression of *IFNB1* and SASP genes. **f**, Treatment with NRTIs rescued CCD. Cells were cultured in medium containing 4 μM abacavir or 1 μM zidovudine. **g**, Treatment with NRTIs repressed the expression of *IFNB1* and SASP genes. **h**, Western blot showing reduced STING dimers in BMR cells treated with NRTIs. **c**,**d**,**h**, The experiments were repeated three times independently with similar results. **i**, In dying BMR cells, cGAS-bound DNA is enriched with B1 and L1 retrotransposons. Immunoprecipitation of cGAS from young and dying BMR cells showed an average of nine- and 19-fold enrichment for B1 and L1 DNA, respectively. The abundance of cGAS-bound DNA was normalized to 5S ribosomal DNA. **e**,**g**,**i**, $n = 3$ technical replicates. **j**, FISH showing the accumulation of B1 and L1 cDNA in the cytoplasm before CCD, which is abrogated by NRTI treatment. Scale bar, 5 μM. **k**, Levels of B1- and L1-cDNA-positive cells. Fluorescence foci-positive cells from four random areas were counted. **b**,**e**,**g**,**i**,**k**, Data are the mean ± s.d. ** $P < 0.01$ and *** $P < 0.001$; unpaired two-sided Student's *t*-test.

through fluorescence in situ hybridization (FISH) using probes against consensus SINE B1 and L1 of BMR. The cytoplasmic B1 and L1 cDNA was abrogated by treatment with NRTIs (Fig. 4j,k). Collectively, these results suggest that activated RTEs in dying BMR cells are responsible for cytoplasmic RNA–DNA hybrid-induced CCD via the cGAS–STING–IFN pathway.

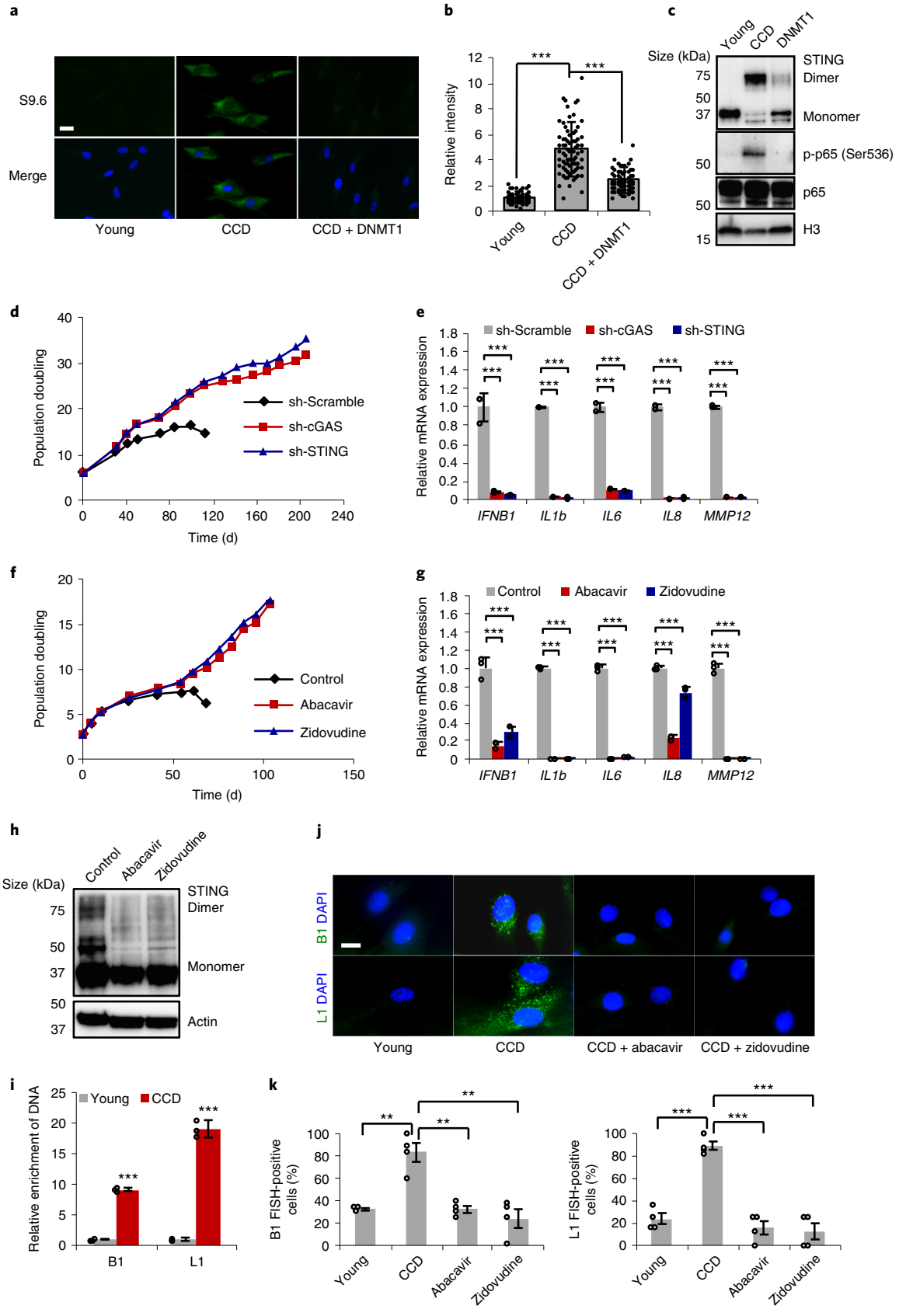

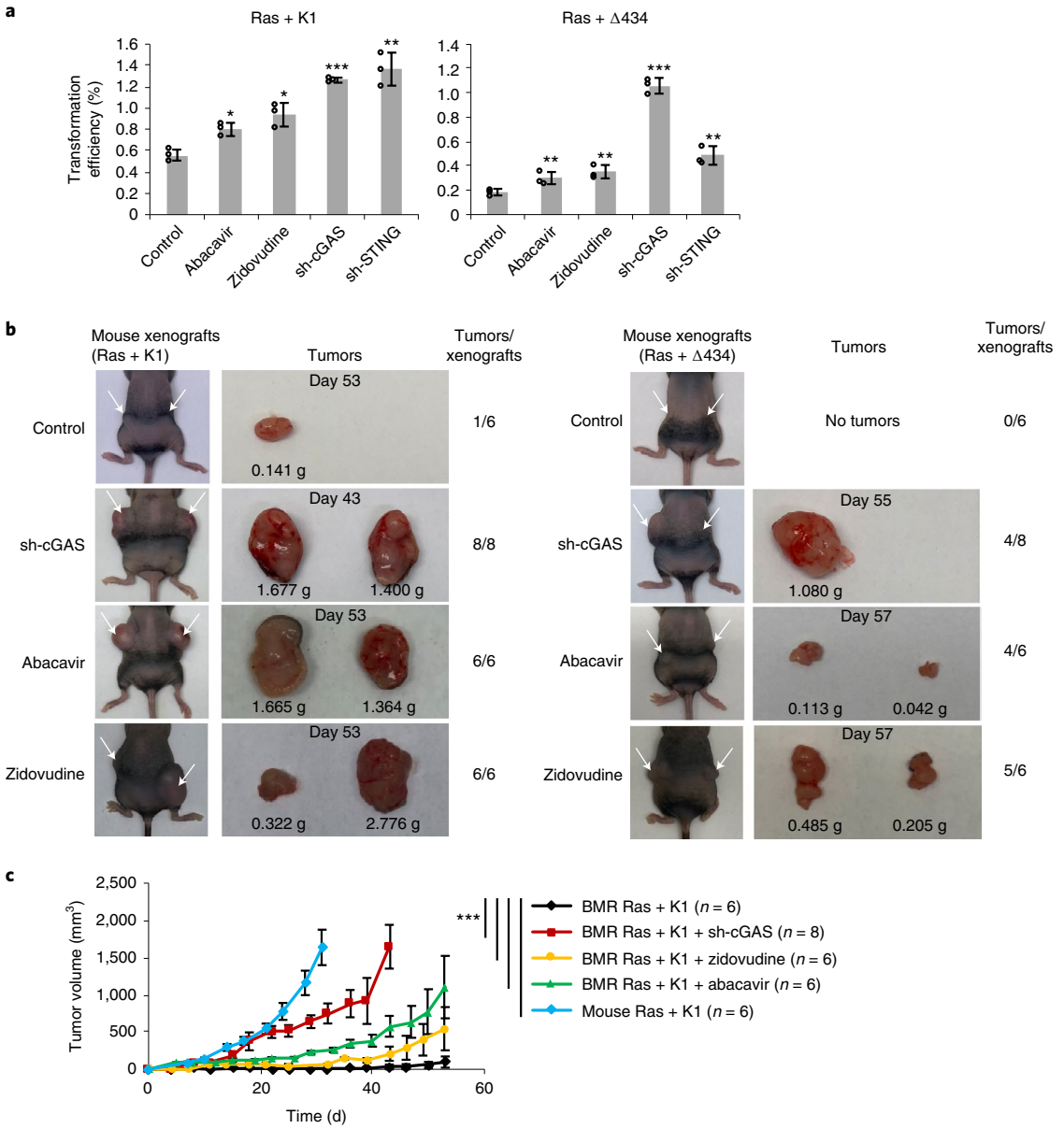

Fig. 5 | Treatment with NRTIs or the knockdown of *cGAS* or *STING* enhances the malignant transformation of BMR cells. a, Soft-agar assays of anchorage-independent growth. BMR cells were transfected with the SV40 LT mutant derivatives K1 (left) or Δ434 (right) and Ras, and plated in soft agar. The cells were cultured in soft agar for 4 weeks, and the colonies were stained and counted. For the NRTI groups, the cells were cultured in soft agar containing 4 μM abacavir or 1 μM zidovudine. The efficiency of transformation was calculated as: number of colonies / (number of seeded cells × transfection efficiency). The experiments were repeated three times. Data are the mean ± s.d. **b**, Xenograft experiment in mice using BMR fibroblasts to investigate the effect of *cGAS* knockdown and NRTI treatment. NIH III immunodeficient nude mice were injected with BMR lung fibroblasts expressing Ras and K1 or Δ434 along with either control or shRNA targeting *cGAS*. For the NRTI groups, the mice were treated with 1 mg ml^{-1} abacavir or 0.5 mg ml^{-1} zidovudine in their drinking water. Transformed mouse cells were injected as a positive control. The cells were allowed to grow for 8 weeks or until the tumors reached 20 mm in the longest dimension. Images of the injected mice and the excised tumors as well as the weight and number of tumors are shown. **c**, Growth curve of the tumors. The volume of the tumor (in mm^3) was calculated as $D \times d \times d / 2$, where D and d are the longest and shortest diameter of the tumors (in mm), respectively. Data are the mean ± s.e.m. **a**,**c**, $^*P < 0.05$, $^{**}P < 0.01$, $^{***}P < 0.001$; unpaired two-sided Student's *t*-test (**a**) or two-way analysis of variance (ANOVA; **c**).

The RTE–cGAS–STING pathway suppresses tumor growth in the BMR. We then tested whether the activated RTEs–cGAS–STING pathway in BMR cells is responsible for the cancer resistance of BMRs. The SV40 LT antigen is an oncoprotein that inactivates two major tumor suppressor pathways, p53 and Rb. LT has two mutant derivatives: LTK1 (K1), which inactivates only p53, and LTΔ434–444 (Δ434), which inactivates only Rb and its family members[36]. Mouse cells can be malignantly transformed with high efficiency by a combination of H-Ras V12 (Ras) and either K1 or Δ434 (ref. [37]). However, BMR cells require inactivation of both p53 and Rb for efficient transformation[37]. To test the role of the RTE–cGAS–STING pathway in BMR resistance to malignant transformation, we transfected BMR fibroblasts with Ras combined with either K1 or Δ434 and cultured them in soft agar with or without the presence of the NRTIs abacavir and zidovudine. Consistent with the previous observations, the combination of Ras with either K1 or Δ434

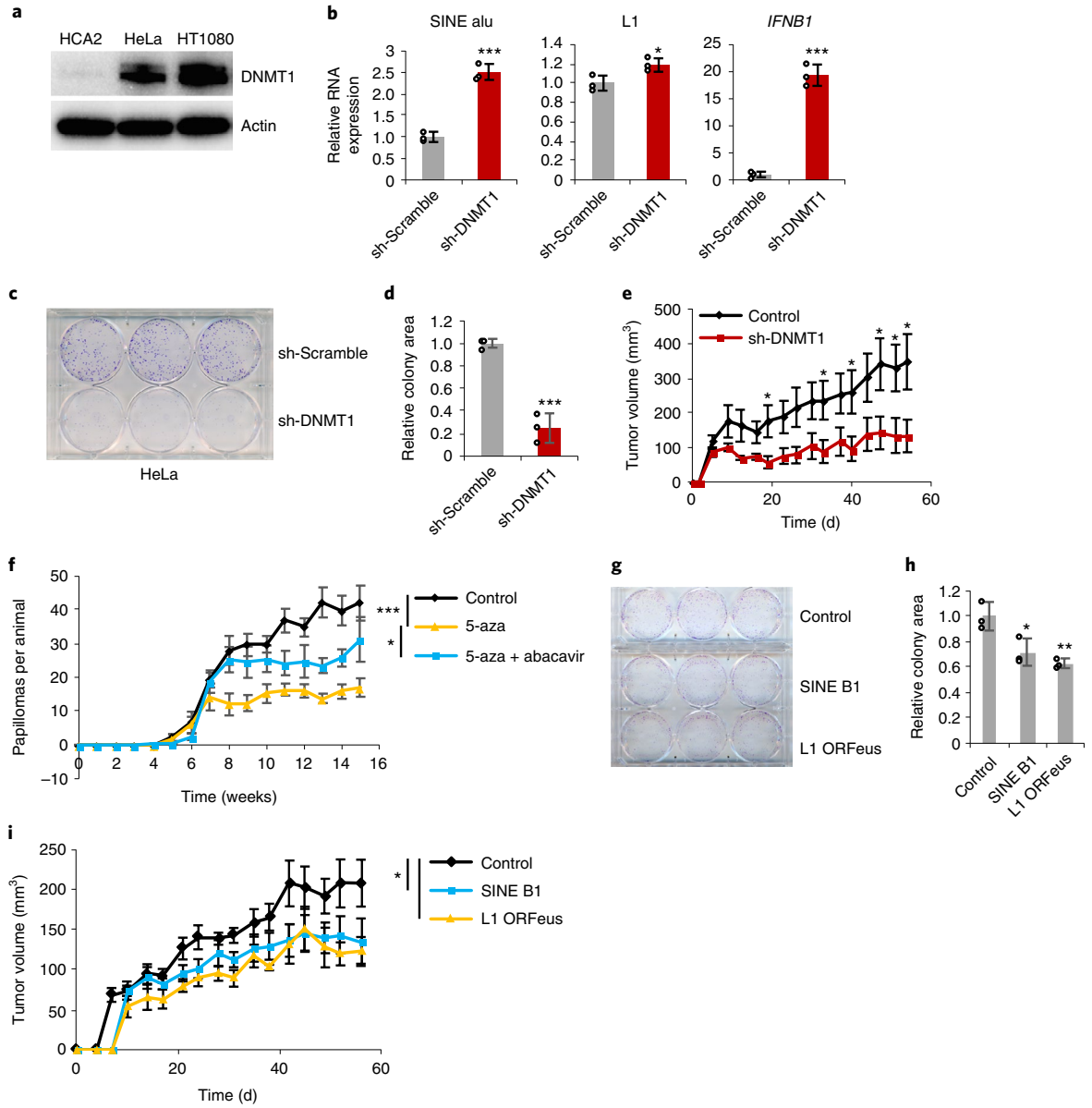

Fig. 6 | Transposons can act as tumor suppressors. a, Western blot showing higher expression of DNMT1 in the cancer cell lines HeLa and HT1080 than primary human skin fibroblasts (HCA2). **b**, Knockdown of *DNMT1* (sh-DNMT1) in HeLa cells elevated the expression (determined by RT–qPCR) of the human retrotransposons SINE Alu and L1, and the *IFNB1* gene. **c**,**d**, Knockdown of *DNMT1* repressed the proliferation of HeLa cells in vitro. A clonogenic assay was performed with crystal violet staining and the colonies areas were quantified. **e**, Knockdown of DNMT1 inhibited the proliferation of HeLa cells in xenografts into nude mice; $n = 6$ independent xenograft injections. **f**, The demethylation reagent 5-Aza repressed DMBA–TPA-induced tumorigenesis, which was restored by NRTI treatment. The experiment was performed using five animals in each group. **g**,**h**, Clonogenic assay showing repressed proliferation of HeLa cells overexpressing SINE B1 and L1. HeLa cells were stably transfected with a SINE B1 or a codon-optimized human L1 (ORFeus) and subjected to a clonogenic assay with crystal violet (**g**); the colony areas were then determined (**h**). **a**–**d**,**g**,**h**, The experiments were repeated three times independently with similar results. **b**,**d**,**h**, $n = 3$ technical replicates. **i**, Overexpression of B1 and L1 repressed the proliferation of HeLa cells in xenografts into nude mice; $n = 6$ independent xenograft injections. **b**,**d**,**e**,**f**,**h**,**i**, Data are the mean ± s.d. (**b**,**d**,**h**) or mean ± s.e.m. (**e**,**f**,**i**). $^{*}P < 0.05$, $^{**}P < 0.01$, $^{***}P < 0.001$; two-sided Student's *t*-test (**b**,**d**,**e**,**h**) or two-way ANOVA (**f**,**i**).

yielded only a small number of colonies in soft agar. However, treatment with either abacavir or zidovudine significantly enhanced proliferation for both Ras + K1 and Ras + Δ434 cells in soft agar (Fig. 5a). Furthermore, knockdown of either *cGAS* or *STING* dramatically increased proliferation (Fig. 5a). These results suggest that NRTI treatment and *cGAS*/*STING* knockdown make BMR cells susceptible to malignant transformation.

We performed a xenograft experiment to further confirm this finding in vivo. We generated BMR cell lines harboring Ras with either K1 or Δ434 and stable knockdown of *cGAS* using shRNA lentivirus. The cells were injected into immunodeficient nude mice and allowed to grow for 8 weeks. For the NRTI treatments, the mice were given abacavir or zidovudine in their drinking water. For cells expressing Ras + K1 with control shRNA, only one of six injections resulted in a small tumor, whereas all injections in the groups of mice that were injected with *cGAS*-knockdown cells or treated with NRTIs resulted in the development of large tumors (Fig. 5b,c). For Ras + Δ434, no tumors were formed with control shRNA, and four

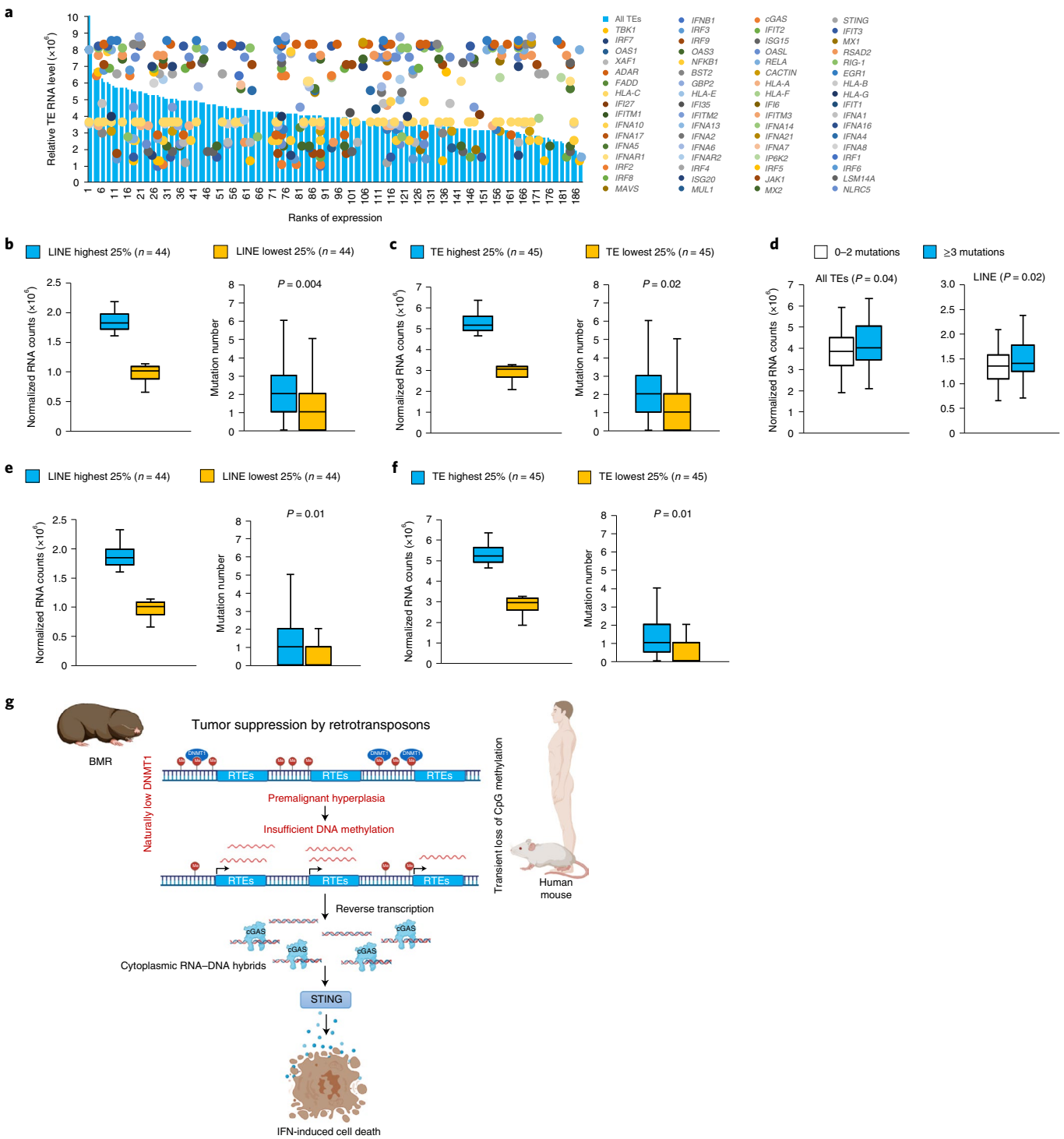

Fig. 7 | Cancer cells with higher expression levels of TEs tend to carry more mutations in genes of the type I IFN pathway. a, Correlation of the levels of TE expression and number of mutations in genes of the type I IFN pathway in cancer cell lines. The expression levels of the TEs were extracted from the RNA-seq data of 188 lung cancer cell lines from the CCLE database. The cell lines were sorted according to the level of TE expression and the mutations of each gene from each cell line were plotted. **b**,**c**, Analysis of the correlation between the expression levels of LINE (**b**) and all TEs (**b**) and the numbers of mutations in genes of the type I IFN pathway (from the CCLE database). Cell lines with the highest and lowest 25% of expression of LINE (**b**) and all TEs (**c**) were grouped (left) and the corresponding mutation numbers were plotted (right). **d**, Lung cancer cell lines with ≥3 mutations in genes of the IFN pathway have higher expression of all TEs and LINEs than cell lines with 0–2 mutations. **e**,**f**, Analysis of the correlation between LINE and all TEs expression levels, and the number of mutations in genes that are directly involved in the IFN pathway and positively regulate or are regulated by IFN. The number of mutations in cell lines with the highest and lowest 25% expression of LINE (**e**) and all TEs (**f**) were plotted. **b**–**f**, The center lines in the boxplots represent the median, the bounds of the box indicate the 1st and 3rd quartiles, and the whiskers indicate 1.5× the interquartile above the third quartile or below the first quartile. The *P* values were determined using an unpaired two-sided Student's *t*-test. **g**, Model of BMR cancer resistance and its generalization to humans and mice. The BMR has naturally low DNMT1. A loss of DNA methylation activates RTEs in hyperplastic cells. Similarly, a transient loss of DNA methylation in hyperplastic lesions in humans and mice also activates RTEs. Activated RTEs form cytoplasmic RNA–DNA hybrids that trigger the cGAS–STING–IFN pathway, which kills premalignant cells.

of eight injections of *cGAS*-knockdown cells, four of six injections in the abacavir treatment group and five of six injections in the zidovudine treatment group formed tumors (Fig. 5b). These results suggest the critical role of the RTE–cGAS–STING pathway in BMR cancer resistance.

RTEs function as tumor suppressors in humans and mice. Demethylating agents have been reported to trigger death of human cancer cells via activation of RTEs and nucleic-acid sensors[24,38]. It is possible that, as a normal tumor-suppressor mechanism, DNMT1 activity becomes limiting during hyperplasia, and this triggers the activation of RTEs in premalignant cells. Notably, DNMT1 is overexpressed in malignant tumors that escape this barrier to transformation[39]. To test whether the mechanism identified in the BMR applies broadly to other mammals, we used two common human cell lines, HeLa and HT1080. Compared with primary human skin fibroblasts, both the HeLa and HT1080 cell lines had significantly higher levels of DNMT1 protein (Fig. 6a). Knockdown of DNMT1 (Extended Data Fig. 7a) activated the expression of SINE Alu (the human homolog of rodent SINE B1), L1 and *IFNB1* (Fig. 6b). The proliferation of both HeLa and HT1080 cells was repressed by DNMT1 knockdown, as determined using a clonogenic assay (Fig. 6c,d and Extended Data Fig. 7b,c). Xenograft experiments in nude mice confirmed that the tumor growth of HeLa cells was repressed by DNMT1 knockdown (Fig. 6e). We next investigated whether, like in the BMR, RTEs serve as tumor suppressors in mice. As many inbred mouse strains carry a nonfunctional *MX1* allele, a gene important for CCD in BMR (Fig. 1e,f), we used a hairless immunocompetent outbred SKH1 mouse strain[40]. The mice were subjected to DMBA–TPA-induced tumorigenesis. When abacavir was administered to the mice in their drinking water, the number of DMBA–TPA-induced papillomas was lower than the control group (Extended Data Fig. 7d). This could be due to side-effects of NRTIs, including anti-angiogenesis and inhibition of telomerase. Meanwhile, the abundant endogenous DNMT1 in mouse tissues may have inhibited the activation of RTEs. We therefore injected the mice with the demethylating agent 5-aza-2′-deoxycytidine (5-Aza) and then administered DMBA–TPA treatment. The mice that were treated with 5-Aza had dramatically lower numbers of papillomas (Fig. 6f). Strikingly, when abacavir was administered in combination with 5-Aza, the papilloma numbers were increased (Fig. 6f and Extended Data Fig. 7e). This result suggests that the protective role of demethylation against tumorigenesis depends largely on the activation of RTEs, particularly L1.

We next tested whether RTEs directly inhibit cancer-cell proliferation. HeLa cells were stably transfected with either the SINE B1 sequence or a codon-optimized L1 (ORFeus). Both B1 and L1 overexpression activated IFNB1 (Extended Data Fig. 7f–h). Clonogenic assays and xenograft experiments showed that both B1 and L1 overexpression inhibited HeLa cell proliferation in vitro and in vivo (Fig. 6g–i). These results suggest that RTEs can exhibit a tumor-suppressive effect in human and mouse cells.

Cancer cells with high levels of RTEs carry more IFN pathway mutations. A seemingly contradictory observation is that many cancer cells have high expression levels of RTEs, including L1. We hypothesized that in established tumors, the IFN pathway is mutated, which allows for unabated RTE activation. To test this, we analyzed the RNA-seq data of 188 lung cancer cell lines from the CCLE database for correlations between the expression levels of different families of TEs using TEtranscripts[41] and mutations in a total of 73 genes from the type I IFN pathway plus cGAS, STING and NF-κB genes (Fig. 7a and Supplementary Data 1). Cell lines in the top 25% of LINE expression had significantly more mutations in genes in the IFN pathway than the bottom 25% (Fig. 7b). A similar result was obtained when the top 25% of all RTE expression was compared with the bottom 25% (Fig. 7c). Alternatively, when the cell lines were grouped based on mutation numbers, the average expression levels of both LINE and RTEs were significantly higher in the cell lines with three or more mutations in genes in the IFN pathway (Fig. 7d). When we further narrowed the gene list down to only the genes that are directly involved in and enhance or are enhanced by IFN (Supplementary Data 1), the result remained the same (Fig. 7e–g). These results confirm that in human cancers high RTE expression is associated with mutations in the IFN pathway.

Discussion

Our study uncovered an anticancer mechanism in a tumor-resistant rodent, the BMR. We showed that a naturally low expression of DNMT1 in the BMR fails to maintain DNA methylation on RTEs during rapid cell proliferation. This results in derepression of RTEs, which form cytoplasmic RNA–DNA hybrids, and trigger an IFN response through the nucleic-acid sensing cGAS–STING pathway. This mechanism eliminates hyperplastic premalignant cells and prevents cancer progression.

Interestingly, genome-wide analysis revealed that the TEs constitute 43.9% of the BMR genome. This percentage is similar to that of humans (45%) and higher than other rodents, including mice (37.5%) and rats (40%)[8,42,43]. This higher percentage of TEs may enhance the anticancer activity of the RTEs in the BMR. A possible reason for BMR adopting a weak DNMT1 as an anticancer strategy is that it carries a mutant *p53* gene. The BMR inhabits subterranean burrows, enduring extreme hypoxia. The p53 of the BMR carries an Arg174Lys mutation mimicking a human tumor mutation[44]. This mutation abrogated its pro-apoptotic activity as an adaptation to hypoxia-induced cell death. As p53 restrains transposons, this mutant p53 in the BMR may have unleashed the transposition. This can also partly explain the reason of the TE expansion in the BMR genome. We hypothesize that the low levels of DNMT1 have co-evolved with the mutant p53 and expanded TEs to trigger the IFN pathway in overproliferating cells, acting as a compensatory strategy.

Persistent activation of RTEs can cause mutations and inflammation, and therefore needs to be tightly regulated. In mammals, multiple mechanisms have evolved to repress transposons, including DNA methylation, heterochromatin, small RNAs and KRAB zinc-finger proteins[5,45]. DNMT1 is responsible for the maintenance of DNA methylation[14,15]. After DNA replication, DNMT1 scans the genome to methylate hemi-methylated regions[46]. Most cells in somatic tissues are in the G0 phase and only occasionally proliferate in response to extrinsic stimuli, including wound healing. The naturally weak DNMT1 in BMRs provides sufficient function for the normal cells but becomes limiting following fast proliferation and hyperplasia. In this way, only hyperplastic cells lose methylation and activate RTEs triggering a suicidal IFN response. In vivo this response may be limited to the vicinity of the pre-neoplastic lesion as IFN acts in a paracrine manner. In addition, IFN-related genes are repressed in normal BMR tissues, as revealed by our transcriptomic analysis, which can further prevent unintended activation of IFN in the BMR.

It has been shown in human cancer cells that DNA-demethylating agents activate ERVs, another type of RTE, which form dsRNA[24,38]. The dsRNA-sensing pathway is an inducer of IFN, as demonstrated in Alu-derived dsRNA[47], and the loss of ADAR, a dsRNA-editing enzyme in cancer cells[48]. However, L1 activation in both humans and mice triggers an IFN response via the cytoplasmic DNA–cGAS–STING pathway[16,17], suggesting that activation of the cGAS–STING pathway by cytoplasmic DNA is a common feature of non-long-terminal-repeat elements in BMRs, mice and humans. In our study we did not observe increased dsRNA during CCD, but only RNA–DNA hybrids. Consistent with this, knockdown of the dsRNA sensors TLR3, MAVs, MDA-5 and RIG-1 failed to rescue CCD. This

is possibly due to the expansion of SINEs in the BMR genome[42] combined with the dramatic derepression of L1. During CCD, both long-terminal-repeat RTEs (ERVs) and non-long-terminal-repeat RTEs (LINEs and SINEs) are activated; but the upregulated LINEs and SINEs have higher basal levels and are more abundant, and thus may provide greater biological influence. This does not exclude the possibility of additional roles played by other types of TEs in BMR cancer resistance.

Strikingly, although enhanced in the BMR, we found this mechanism is also applicable to humans and mice. DNMT1 tends to be overexpressed in malignant tumors that escaped the barrier to transformation[39]. This was also confirmed in our experiments with human cancer cells. Knockdown of DNMT1 in human cancer cells triggered a similar response to that in BMR cells during CCD, including elevated SINEs and L1, induction of IFN and reduced cell proliferation in vitro and in vivo. Similarly, mice treated with the DNMT1 inhibitor 5-Aza dramatically repressed papillomas induced by DMBA–TPA. This repression is at least partly due to activated RTEs, which was confirmed by the restoration of papillomas by NRTI treatment. Notably, treating the mice with NRTI alone did not increase papillomas; instead, NRTI treatment reduced papillomas. This is possibly because NRTI has some anticancer effects through the inhibition of telomerase (another type of reverse transcriptase in cells)[49] and anti-angiogenesis[50–52]. These results suggest that the role of RTEs as tumor suppressors is not limited in the BMR but is applicable to other mammals.

It has been argued that RTEs are highly expressed in some cancer cells and thus RTEs drive carcinogenesis[53]. We showed that more genes in the IFN pathway were mutated in cancer cell lines with higher expression levels of RTEs. Therefore, the selective pressure against RTE activation had been lost in these cancer cells. Interestingly, the p53 tumor suppressor, which is lost or mutated in over 50% of human cancers, represses RTEs[54]. Thus, RTE-mediated cell death can provide a back-up barrier to stop proliferation for cells that have lost p53.

Retrotransposable elements are selfish elements that are highly abundant in mammalian genomes, where they may acquire functional roles through 'domestication'[55]. Here we propose that TEs were co-opted to serve as tumor suppressors by gauging cell overproliferation and triggering the death of hyperplastic cells via the activation of cytoplasmic nucleic-acid sensors. This finding assigns a new beneficial function to RTEs and may explain why mammalian genomes have not eliminated these elements. Interestingly, other anticancer mechanisms, such as apoptosis[56,57] and cellular senescence[58,59], display antagonistic pleiotropy, where they contribute to aging pathologies in late life. Similarly, persistent RTE activation contributes to aging by promoting sterile inflammation[16,17]. However, as derepressed RTEs in aging is not specific to tumors, age-related activation of RTEs does little to reduce the risk of cancer in the elderly. In addition, other pro-tumorigenic changes that occur with age, such as metabolic changes and the accumulation of mutations, may overpower the tumor-suppressive effect of RTEs.

Our study points to RTE activation as a useful target for cancer treatment. In addition, NRTIs are broadly used as antivirals for HIV treatment or prevention. Although the benefits of NRTIs clearly outweigh the risks in HIV patients, our study suggest that potential cancer risks associated with NRTIs warrant further investigation when NRTIs are chronically administered to healthy people. In summary, our study demonstrates that the study of animals that are naturally cancer resistant provides a strategy for the identification of mechanisms broadly applicable to humans.

Online content

Any methods, additional references, Nature Research reporting summaries, source data, extended data, supplementary information, acknowledgements, peer review information; details of author contributions and competing interests; and statements of data and code availability are available at https://doi.org/10.1038/s41590-021-01027-8.

Received: 27 April 2021; Accepted: 11 August 2021;
Published online: 23 September 2021

References

1. Seluanov, A., Gladyshev, V. N., Vijg, J. & Gorbunova, V. Mechanisms of cancer resistance in long-lived mammals. *Nat. Rev. Cancer* **18**, 433–441 (2018).
2. Gorbunova, V. et al. Cancer resistance in the blind mole rat is mediated by concerted necrotic cell death mechanism. *Proc. Natl Acad. Sci. USA* **109**, 19392–19396 (2012).
3. Manov, I. et al. Pronounced cancer resistance in a subterranean rodent, the blind mole-rat, *Spalax*: in vivo and in vitro evidence. *BMC Biol.* **11**, 91 (2013).
4. Nevo, E. *Mosaic Evolution of Subterranean Mammals: Regression, Progression, and Global Convergence* (Oxford Univ. Press, 1999).
5. Bourque, G. et al. Ten things you should know about transposable elements. *Genome Biol.* **19**, 199 (2018).
6. Lander, E. S. et al. Initial sequencing and analysis of the human genome. *Nature* **409**, 860–921 (2001).
7. Mouse Genome Sequencing Consortium. Initial sequencing and comparative analysis of the mouse genome. *Nature* **420**, 520–562 (2002).
8. Pace, J. K. 2nd & Feschotte, C. The evolutionary history of human DNA transposons: evidence for intense activity in the primate lineage. *Genome Res.* **17**, 422–432 (2007).
9. Gasior, S. L., Wakeman, T. P., Xu, B. & Deininger, P. L. The human LINE-1 retrotransposon creates DNA double-strand breaks. *J. Mol. Biol.* **357**, 1383–1393 (2006).
10. Iskow, R. C. et al. Natural mutagenesis of human genomes by endogenous retrotransposons. *Cell* **141**, 1253–1261 (2010).
11. Gilbert, N., Lutz-Prigge, S. & Moran, J. V. Genomic deletions created upon LINE-1 retrotransposition. *Cell* **110**, 315–325 (2002).
12. Slotkin, R. K. & Martienssen, R. Transposable elements and the epigenetic regulation of the genome. *Nat. Rev. Genet.* **8**, 272–285 (2007).
13. Leonova, K. I. et al. p53 cooperates with DNA methylation and a suicidal interferon response to maintain epigenetic silencing of repeats and noncoding RNAs. *Proc. Natl Acad. Sci. USA* **110**, E89-98 (2013).
14. Li, E., Bestor, T. H. & Jaenisch, R. Targeted mutation of the DNA methyltransferase gene results in embryonic lethality. *Cell* **69**, 915–926 (1992).
15. Robert, M. F. et al. DNMT1 is required to maintain CpG methylation and aberrant gene silencing in human cancer cells. *Nat. Genet.* **33**, 61–65 (2003).
16. De Cecco, M. et al. L1 drives IFN in senescent cells and promotes age-associated inflammation. *Nature* **566**, 73–78 (2019).
17. Simon, M. et al. LINE1 derepression in aged wild-type and SIRT6-deficient mice drives inflammation. *Cell Metab.* **29**, 871–885 (2019).
18. Fukuda, S. et al. Cytoplasmic synthesis of endogenous *Alu* complementary DNA via reverse transcription and implications in age-related macular degeneration. *Proc. Natl Acad. Sci. USA* **118**, e2022751118 (2021).
19. Lee, E. et al. Landscape of somatic retrotransposition in human cancers. *Science* **337**, 967–971 (2012).
20. Helman, E. et al. Somatic retrotransposition in human cancer revealed by whole-genome and exome sequencing. *Genome Res.* **24**, 1053–1063 (2014).
21. Tubio, J. M. C. et al. Mobile DNA in cancer. Extensive transduction of nonrepetitive DNA mediated by L1 retrotransposition in cancer genomes. *Science* **345**, 1251343 (2014).
22. Miki, Y. et al. Disruption of the *APC* gene by a retrotransposal insertion of L1 sequence in a colon cancer. *Cancer Res.* **52**, 643–645 (1992).
23. Burns, K. H. Our conflict with transposable elements and its implications for human disease. *Annu Rev. Pathol.* **15**, 51–70 (2020).
24. Chiappinelli, K. B. et al. Inhibiting DNA methylation causes an interferon response in cancer via dsRNA including endogenous retroviruses. *Cell* **162**, 974–986 (2015).
25. Sheng, W. et al. LSD1 ablation stimulates anti-tumor immunity and enables checkpoint blockade. *Cell* **174**, 549–563 (2018).
26. Gu, Z. et al. Silencing of LINE-1 retrotransposons is a selective dependency of myeloid leukemia. *Nat. Genet.* **53**, 672–682 (2021).
27. Numajiri, A., Mibayashi, M. & Nagata, K. Stimulus-dependent and domain-dependent cell death acceleration by an IFN-inducible protein, human MxA. *J. Interferon Cytokine Res.* **26**, 214–219 (2006).
28. Harada, H. et al. Absence of the type I IFN system in EC cells: transcriptional activator (IRF-1) and repressor (IRF-2) genes are developmentally regulated. *Cell* **63**, 303–312 (1990).
29. Jin, J. et al. Noncanonical NF-κB pathway controls the production of type I interferons in antiviral innate immunity. *Immunity* **40**, 342–354 (2014).
30. Hou, Y. et al. Non-canonical NF-κB antagonizes STING sensor-mediated DNA sensing in radiotherapy. *Immunity* **49**, 490–503 (2018).

31. Dou, Z. et al. Cytoplasmic chromatin triggers inflammation in senescence and cancer. *Nature* **550**, 402–406 (2017).
32. Quentin, Y. A master sequence related to a free left Alu monomer (FLAM) at the origin of the B1 family in rodent genomes. *Nucleic Acids Res.* **22**, 2222–2227 (1994).
33. Slack, A., Cervoni, N., Pinard, M. & Szyf, M. DNA methyltransferase is a downstream effector of cellular transformation triggered by simian virus 40 large T antigen. *J. Biol. Chem.* **274**, 10105–10112 (1999).
34. Mankan, A. K. et al. Cytosolic RNA:DNA hybrids activate the cGAS–STING axis. *EMBO J.* **33**, 2937–2946 (2014).
35. Dai, L., Huang, Q. & Boeke, J. D. Effect of reverse transcriptase inhibitors on LINE-1 and Ty1 reverse transcriptase activities and on LINE-1 retrotransposition. *BMC Biochem.* **12**, 18 (2011).
36. Hahn, W. C. et al. Enumeration of the simian virus 40 early region elements necessary for human cell transformation. *Mol. Cell. Biol.* **22**, 2111–2123 (2002).
37. Tian, X. et al. Evolution of telomere maintenance and tumour suppressor mechanisms across mammals. *Philos. Trans. R Soc. B* **373**, 20160443 (2018).
38. Roulois, D. et al. DNA-demethylating agents target colorectal cancer cells by inducing viral mimicry by endogenous transcripts. *Cell* **162**, 961–973 (2015).
39. Zhang, W. & Xu, J. DNA methyltransferases and their roles in tumorigenesis. *Biomark. Res.* **5**, 1 (2017).
40. Schaffer, B. S. et al. Immune competency of a hairless mouse strain for improved preclinical studies in genetically engineered mice. *Mol. Cancer Ther.* **9**, 2354–2364 (2010).
41. Jin, Y., Tam, O. H., Paniagua, E. & Hammell, M. TEtranscripts: a package for including transposable elements in differential expression analysis of RNA-seq datasets. *Bioinformatics* **31**, 3593–3599 (2015).
42. Fang, X. et al. Genome-wide adaptive complexes to underground stresses in blind mole rats *Spalax*. *Nat. Commun.* **5**, 3966 (2014).
43. Gibbs, R. A. et al. Genome sequence of the Brown Norway rat yields insights into mammalian evolution. *Nature* **428**, 493–521 (2004).
44. Ashur-Fabian, O. et al. Evolution of p53 in hypoxia-stressed *Spalax* mimics human tumor mutation. *Proc. Natl Acad. Sci. USA* **101**, 12236–12241 (2004).
45. Imbeault, M., Helleboid, P. Y. & Trono, D. KRAB zinc-finger proteins contribute to the evolution of gene regulatory networks. *Nature* **543**, 550–554 (2017).
46. Schneider, K. et al. Dissection of cell cycle-dependent dynamics of Dnmt1 by FRAP and diffusion-coupled modeling. *Nucleic Acids Res.* **41**, 4860–4876 (2013).
47. Mehdipour, P. et al. Epigenetic therapy induces transcription of inverted SINEs and ADAR1 dependency. *Nature* **588**, 169–173 (2020).
48. Liu, H. et al. Tumor-derived IFN triggers chronic pathway agonism and sensitivity to ADAR loss. *Nat. Med.* **25**, 95–102 (2019).
49. Leeansyah, E. et al. Inhibition of telomerase activity by human immunodeficiency virus (HIV) nucleos(t)ide reverse transcriptase inhibitors: a potential factor contributing to HIV-associated accelerated aging. *J. Infect. Dis.* **207**, 1157–1165 (2013).
50. Song, L. et al. Nucleoside/nucleotide reverse transcriptase inhibitors attenuate angiogenesis and lymphangiogenesis by impairing receptor tyrosine kinases signalling in endothelial cells. *Br. J. Pharm.* **175**, 1241–1259 (2018).
51. Barillari, G. The anti-angiogenic effects of anti-human immunodeficiency virus drugs. *Front. Oncol.* **10**, 806 (2020).
52. Armando, R. G., Mengual Gomez, D. L. & Gomez, D. E. New drugs are not enough—drug repositioning in oncology: an update. *Int. J. Oncol.* **56**, 651–684 (2020).
53. Ting, D. T. et al. Aberrant overexpression of satellite repeats in pancreatic and other epithelial cancers. *Science* **331**, 593–596 (2011).
54. Wylie, A. et al. p53 genes function to restrain mobile elements. *Genes Dev.* **30**, 64–77 (2016).
55. Jangam, D., Feschotte, C. & Betran, E. Transposable element domestication as an adaptation to evolutionary conflicts. *Trends Genet.* **33**, 817–831 (2017).
56. Matheu, A., Maraver, A. & Serrano, M. The Arf/p53 pathway in cancer and aging. *Cancer Res.* **68**, 6031–6034 (2008).
57. Tyner, S. D. et al. p53 mutant mice that display early ageing-associated phenotypes. *Nature* **415**, 45–53 (2002).
58. Coppe, J. P. et al. Senescence-associated secretory phenotypes reveal cell-nonautonomous functions of oncogenic RAS and the p53 tumor suppressor. *PLoS Biol.* **6**, 2853–2868 (2008).
59. Campisi, J. & d'Adda di Fagagna, F. Cellular senescence: when bad things happen to good cells. *Nat. Rev. Mol. Cell Biol.* **8**, 729–740 (2007).

Methods

Animals. Compliance with ethical regulations and all animal experiments were approved by the University Committee on Animal Resources of the University of Rochester. The BMRs (*Spalax galili*) were wild caught from the Upper Eastern Galilee Mountains in Israel and housed individually. C57BL/6 mice of both genders were purchased from Taconic Biosciences, Inc. NIH III nude (Crl:NIH-Lyst$^{bg\text{-}J}$Foxn1^{nu}Btk^{xid}) and SKH1 hairless (Crl:SKH1-Hrhr) mice were purchased from Charles River Laboratories Inc.

Cell culture. Primary fibroblasts were isolated from lung and skin tissue of at least three BMRs and three mice. All of the BMR fibroblast cell lines have similar growth characteristics and occurrence of CCD. The human primary skin fibroblasts HCA2 were a gift from O. Pereira-Smith. The fibroblasts were maintained in EMEM media (ATCC) with 15% (vol/vol) fetal bovine serum (FBS) on treated polystyrene culture dishes (Corning) in a 37 °C incubator in an atmosphere of 5% CO_2 and 3% O_2. HeLa and HT1080 cells were cultured in DMEM medium (Gibco) with 10% (vol/vol) FBS. For all cell cultures, 100 μg ml^{-1} penicillin and 100 U ml^{-1} streptomycin (Gibco) were added.

Plasmids and lentivirus. Complementary DNA of human DNMT1; SV40 LT, K1 and Δ434; and codon-optimized L1(ORFeus) were PCR amplified from the corresponding plasmids (Addgene) and subcloned into a pPB expression vector under the CAG promoter. For overexpression, all pPB plasmids were co-transfected with a pPB transposase (pBase) plasmid, followed by puromycin selection. The pWZL-hygro-H-Ras V12 (Addgene, 18749) plasmid was linearized using NotI before transfection, to enhance the genomic integration, followed by hygromycin selection. For B1 overexpression, consensus sequence of mouse SINE B1 was ligated into a pPB shRNA vector. The SINE B1 RNA will be expressed by the H1 promoter of the vector without forming shRNA.

For shRNA-mediated knockdown, the following shRNAs against BMR *MX1*, *cGAS* and *STING* were synthesized by Integrated DNA Technology (IDT): *MX1*, TCCACGGAAAGTCAGAAAGAACAGCCTGA; *cGAS*, GACTCTAGACGTGTAAGGACAACTTGGAA; and *STING*, TGCTGTCTGGTTGAAGAACTATGCCACGT. The sequences were ligated into an iLenti-siRNA-GFP lentiviral vector (abm). The lentiviral vectors were co-transfected with the packaging plasmids psPAX2 (Addgene, 12260) and VSV-G (Addgene, 14888) into HEK293T cells. The viral supernatant was collected and filtered through a 0.45 μm filter. To infect target cells, the viral supernatant was supplemented with 8 μg ml^{-1} polybrene and applied to the cells. The infected cells were selected with puromycin.

Transfection. Mouse, human and BMR fibroblasts were seeded at 5×10^5 cells per 10 mm plate and cultured for 5 d before transfection. For transfection, 1×10^6 cells were harvested and transfected with 5 μg plasmid DNA using Amaxa Nucleofector II, program T-020 and NHDF solution (Amaxa). The medium was changed 24 h after transfection to remove the dead cells.

Conditioned media and IFN treatment. For conditioned media, lung or skin fibroblasts of the BMR undergoing CCD were maintained in complete EMEM medium for 5 d. The medium was then collected and centrifuged to remove the cell debris. For BMR IFN-enriched media, human skin fibroblast HCA2 cells were transfected with a pPB expression vector ligated with BMR IFN cDNA and selected with puromycin for 1 week to obtain integrated colonies. Stably transfected cells were pooled and cultured for 5 d. The medium was collected and centrifuged. Conditioned media or IFN-enriched media were applied to young, growing BMR cells mixed with 1×volume of fresh complete EMEM medium to provide sufficient nutrients. After 2 weeks of incubation, the cells were collected for a comet assay.

RT–qPCR. Total RNA from cells and tissues was extracted using a Quick-RNA miniprep kit (Zymo), with a DNase I column digestion to remove genomic DNA contamination. Reverse transcription was performed using an iScript cDNA synthesis kit (Bio-Rad). Quantitative PCR was performed using a CFX Connect real-time PCR detection system (Bio-Rad). The results were normalized to *β-actin*.

To identify the active L1 sequence in BMR, a protein sequence of L1 ORF1 from the mouse L1MdaI family was used as the query to perform a tblastn search against the BMR genome (GCA_000622305.1). As most of the hits harbor ORF-disrupting mutations, a homemade Perl script was used to screen hits without disrupting mutations. Complete ORF1 proteins from these hits were predicted using GeneWise[60] and the corresponding genomic sequence with 2,000-bp flanking sequences and mouse L1MdaI protein sequence. Transcriptome was used to determine the expressed and potentially functional ORF1 proteins in BMR cells. More than 20,000 loci with >1,000 bp sequence covered by transcriptomic reads were selected to predict the ORF1 protein sequences using GeneWise using the corresponding genomic sequence with 6,000-bp flanking sequences and the previously predicted BMR ORF1 protein sequence. As a result, 44 predicted ORF1 protein sequences with at least 200 amino acids were obtained, two of which have highest conservation with mouse L1MdaI.

Primers for SINE B1 and B2 were designed based on rodent consensus sequences obtained from SIENBase. The L1 primers were designed based on the sequence of the two BMR L1 closest to the mouse L1Mda1 ORF1. Primers for all of the other genes were designed according to the annotated corresponding BMR genes crossing exon–intron junctions. The following primers were used: *IFNB1*, ACCTTGCTCCTTCTGTGCT and AACTGCTGTTGGTGCTTGA; *DNMT1*, GAAACCGCCACAACCACTG and ACTCACGCACGCTCACCA; *SINE B1*, CGCCTTTAATCCCAGCAC and GCTGTCCTGGAACTCACT; *SINE B2*, GAGATGGCTCAGTGGGTAA and GCAGAGGTCAGAAGAGGG; *LINE-1*, TCCTCTAGAGACAATGCAGGACA and TCATTCAGAAGTTTATCC; *IL1b*, TGATGCACCCCTTCGACTTC and CAAGGCCACAGGTGTTTTGT; *IL6*, GAACCCTCCATCCTCTTGCC and GGCCTCGTCATTGTTCAAGC; *IL8*, GAACTTCGATGCCAGTGCAAG and CAAAACCCTCTGCACCCACTT; *MMP12*, AGTGCCCGATGTTCAGCATT and AATGTCAGCCTCGCCTTCAT; *P21* (*CDKN1A*), TGGTGTCTCACTCCCCTGAG and CCTCTTAGAGAAGA CCAGCCG; P16 (*CDKN2A*), CATGGAGCGGACCCCAACT and TCCTCAC CTGAGGGAGCTTT; *cGAS* (*MB21D1*), GTCAGACGACTGGAATCCCC and GCCAGGTCTTTGAACTCCGA; *STING* (*TMEM173*), AGCTTGGTGATCC TTTCGGG and GGTACCTGGATTGGACGTGG; *GAPDH*, TGGCCTTCC GTGTTCCTACC and ACCAGAGACAAGCCCAGCTC; and *5S rDNA*, CTCGTCTGATCTCGGAAGCTAAG and GCGGTCTCCCATCCAAGTAC.

5′ RACE. Total RNA was collected from BMR fibroblasts entering CCD. For each reaction, 1 μg total RNA was subjected to the 5′ RACE system (Thermo Fisher, 18374-058). Two antisense gene-specific primers (GSPs) for B1 and L1, respectively, were used: B1-GSP1, TGTAGCCCTGGCTGTCCT and B1-GSP2, CACTATGTAGACCAGGCTGGCC; and L1-GSP1, TCATTCAGAAGTTTATCC and L1-GSP2, ATGTGGGTCAGAAGTTTTCAGACTTTCTCCTTA. The amplification products were ligated into the pCR2.1 vector and transformed into One Shot TOP10 chemically competent *Escherichia coli* (Thermo Fisher, C404010). A total of 60 clones of both B1 and L1 were sequenced by Genewiz using the M13R primer. Multiple alignment with consensus B1 and L1 5′ UTR sequences was performed using Clustal Omega and visualized using Jalview. To predict the consensus start site of the L1 5′ UTR, the genomic regions harboring the L1 5′ UTR were determined using the blastn program using the sequences from the 5′ RACE assays. Genomic sequences 1,000 bp upstream of the top10 blastn hits were extracted and aligned using ClustalW. A highly conserved region (~600 bp) and a short adenine nucleotide-rich region at the 5′ end of this conserved region was observed. This adenine nucleotide-rich region hints that it may contain target site duplication (TSD) sequences. To identify the paired TSD in each L1 copy, 30-bp sequences covering the A polymer were used to search against the 2,000-bp genomic sequences 6,000 bp downstream of the adenine nucleotide-rich region using the blastn program. Paired TSD sequences were successfully identified in six copies with no more than two mismatches and others failed due to the incomplete genomic sequences. Among these six paired TSD sequences, all upstream TSD are followed by a guanine nucleotide and all downstream TSD are preceded by polyA-like sequences, suggesting the histories of L1 retrotransposition. Therefore, we used this highly conserved region following the TSD to infer the 5′ UTR consensus sequence.

Antibodies. The following antibodies were used: anti-DNMT1 (Abcam, ab13537; 1:1,000), anti-cGAS (Millipore, ABF124; 1:1,000 for western blots), anti-STING (Thermo Fisher Scientific, PA5-70420; 1:1,000 for western blots), anti-MX1 (Thermo Fisher Scientific, PA5-22149; 1:1,000 for western blots), anti-p65 (Cell Signaling Technology, 8242; 1:1,000 for western blots), anti-p-p65 Ser536 (Cell Signaling Technology, 3033; 1:1,000 for western blots), anti-Chk2 (Cell Signaling Technology, 2662; 1:1,000 for western blots), anti-p-Chk2 T68 (Cell Signaling Technology, 2661; 1:1,000 for western blots), anti-p53 (Cell Signaling Technology, 2524; 1:500 for western blots), anti-p-p53 S15 (Cell Signaling Technology, 12571; 1:500 for western blots), anti-S9.6 (Kerafast, ENH001; 1:500 for immunofluorescence), anti-J2 (Kerafast, ES2001; 1:60 for immunofluorescence), anti-LINE-1 ORF1p (Millipore, MABC1152; 1:1,000 for western blots) and anti-γH2AX (Millipore, 05-636-I; 1:1,000 for western blots).

Western blots. Western blotting was performed as previously described[61], with slight modifications. Cells were harvested and suspended in PBS with protease inhibitor cocktail (Roche) and then mixed with 1×volume of 2×Laemmli sample buffer (Bio-Rad). The extracts were boiled and centrifuged at 14,000*g* for 15 min at 4 °C. For STING dimers, the cells were harvested and washed three times with PBS. The cell pellets were then incubated with 2 mM disuccinimidyl suberate for 30 min at room temperature before protein extraction. The protein samples were resolved by SDS–PAGE and transferred to PVDF membranes (Bio-Rad). The membranes were blocked with 5% BSA in TBS supplemented with 0.1% Tween 20 and incubated with the indicated primary antibodies. Horseradish peroxidase-conjugated anti-rabbit or anti-mouse IgG (Abcam) secondary antibodies were used. Proteins were visualized using an ECL kit (Bio-Rad). Quantification of bands was performed using ImageJ.

Clonogenic assay. The clonogenic assay was performed according to a previously published protocol[62], with slight modifications. BMR cells were transfected with pPB-DNMT1 and pBase vectors selected with 2 μg ml^{-1} puromycin and allowed to grow for 3 weeks until colonies formed. The colonies were fixed with 10% formalin

for 5 min and then stained with a staining solution containing 0.5% crystal violet and 20% methanol for 5 min. For cancer cells, 500 cells per well were seeded in six-well plates and the cells were cultured for 7 d before staining with crystal violet.

SA-β-gal staining. SA-β-gal staining was performed according to the protocol of the Campisi laboratory[63]. BMR fibroblasts at low and high population doublings were seeded at approximately 40% confluence one day before staining to avoid false-positive staining due to overconfluence. The cells were fixed with 2% formaldehyde and 0.2% glutaraldehyde in PBS for 5 min at room temperature. After two washes with PBS, the cells were stained with a staining solution containing 20 mg ml^{-1} X-gal in dimethylformamide, 0.2 M citric acid/Na phosphate buffer (pH 6.0), 100 mM potassium ferrocyanide, 100 mM potassium ferricyanide, 5 M $NaCl_2$ and 1 M $MgCl_2$. The plates were incubated at 37 °C for 16 h without CO_2. For quantification, images of three different areas from each sample were captured and SA-β-gal staining of at least 100 cells in each area was counted.

Immunofluorescence and FISH. Cells were seeded in wells of chamber slides at a density of 3×10^4 cells per well. One day later, the cells were fixed with 3.7% paraformaldehyde at 37 °C for 15 min and permeabilized with 0.5% Triton X-100 in PBS. For cytoplasmic RNA–DNA hybrids and dsRNA staining, the cells were further incubated with 100% methanol at −20 °C overnight. The cells were then blocked with 5% BSA and 10% FBS in PBS with or without RNase H or RNase III at 37 °C for 4 h and incubated at 4 °C overnight with primary antibodies diluted in blocking reagent. For γH2AX, cells in chamber slides were directly blocked after permeabilization and incubated with primary antibody in blocking reagent. Images were acquired using a Nikon Eclipse Ti-S inverted fluorescence microscope. All microscope exposures were set to below saturation, and the settings were kept constant for all images across all samples in one experiment. Quantification of immunofluorescence intensity was performed using ImageJ.

For FISH, cells in chamber slides were fixed with 4% paraformaldehyde at 37 °C for 10 min and permeabilized with cold methanol for 10 min. The cells were then rehydrated with 70% ethanol for 10 min. After ethanol removal, the cells were treated with 1 mg ml^{-1} RNase A at room temperature for 30 min before 1 M Tris (pH 8.0) was added. After 5 min of Tris treatment, 2 ng μl^{-1} Alexa-488-conjugated probes in hybridization buffer (1 mg ml^{-1} yeast transfer RNA, 0.005% BSA, 10% dextran sulfate, 25% dionized formamide and 2×SSC) were added. The chamber slides were subjected to heat shock at 78 °C for 2 min and allowed to anneal by incubating at 37 °C for 1 h. The sides were washed once with 4×SSC for 5 min, followed by three washes with 2×SSC for 5 min. The slides were sealed with mounting medium containing 4,6-diamidino-2-phenylindole. For BMR B1 and L1 DNA FISH, the following probes were used: B1 probe, TGCACGCCTTTAATCCCAGCACTC–Alexa-488 and L1 probe, TACAAGAAGCCTACAGAACTCCAA–Alexa-488;

Immunoprecipitation of cGAS. Cells were seeded in plates and allowed to grow to 80% confluence. The cells were washed with PBS and crosslinked by 2,500 J m^{-2} ultraviolet (UV) radiation using a Stratolinker UV system. The cells were then lysed using cytoplasmic lysis buffer (50 mM HEPES, 150 mM NaCl, 10% glycerol, 1 mM dithiothreitol, 2 mM EDTA (pH 8.0), and 2.5% digitonin), supplemented with salmon sperm DNA and incubated at 4 °C for 5 min with shaking. The lysates were centrifuged at 12,000*g* for 30 min at 4 °C to remove the nuclei and pre-cleared with 20 μl of agarose A beads with salmon sperm DNA. The cGAS was pulled down by overnight incubation with 5 μg anti-cGAS (Millipore, ABF124), followed by the addition of 30 μl of agarose A beads with salmon sperm DNA and 2 h incubation with rotation. The beads were washed five times with lysis buffer before the DNA was isolated using a Zymo quick-DNA miniprep plus kit. The purified DNA (1 ng) was used as the qPCR template. For B1- and L1-enrichment detection, the qPCR was normalized to *5S rDNA* to control for nuclear DNA contamination during cell fractionation; in addition, qPCR using primers against *GAPDH* was performed to ensure that there was no significant contamination from nuclear genomic DNA.

RNA-seq. Total RNA from early- and late-passage BMR fibroblasts was extracted using a Quick-RNA miniprep kit (Zymo), with a DNase I column digestion to remove genomic DNA contamination. For tissues, five wild-caught mice and five BMRs were perfused with PBS and tissues were collected for total RNA extraction. The RNA samples were processed with the Illumina TruSeq stranded total RNA RiboZero Gold kit and then subjected to Illumina HiSeq 4000 paired-end 150-bp sequencing at the New York University Genome Technology Center. Over 50 million reads per sample were obtained. The RNA-seq experiment was performed in three biological replicates for cells and five biological replicates for tissues.

The RNA-seq reads were first trimmed using Trim_Galore, which trimmed both low-quality base calls and adapter sequences. After the trimming, only reads longer than 50 bp were used for alignment. STAR[64] was used for the alignment of paired-end reads onto the BMR genome (genome sequence and GFF annotation of genes were downloaded from Ensemble, release 91). Only alignment with less than a 4% mismatch (--outFilterMismatchNoverLmax 0.04) were considered. Considering potential multiple instances of TEs, at most 100 multiple alignments were allowed for a read (--outFilterMultimapNmax 100). Genome-wide annotation of TEs was generated using RepeatMasker (v4.07)[65] with RepBase repeat libraries (20170127 (27 January 2017))[66]. With the sequence alignment, it was challenging to accurately evaluate the expression level of each instance of a TE. To overcome this challenge, TEtranscripts[41] was used to measure abundance at the resolution of the element level, combining transcripts of all instances of the same TE. Particularly for B1 TEs, we found the changes in expression levels (between young and CCD cells) were associated with CpG counts, so we divided instances of a TE into subgroups according to CpG counts in each instance. With the estimated read counts of genes and TEs from TEtranscripts, DESeq2 (ref. [67]) was used for differential analysis. During differential analysis, simple repeats, low complexity and rRNA TEs were ignored, and TEs with FDR < 0.01 and fold change > 1.5 were considered differentially expressed between young and CCD cells. Genes with a fold change > 10 were considered the most upregulated genes and were used for Gene ontology term and pathway enrichment analysis. For comparisons of BMR and mouse tissues, high-confident one-to-one orthologs (15,137 protein-coding genes) between BMR and mouse were obtained from Ensembl BioMart (release 101)[68]. All of the BMR genes tagged as high mouse orthology confidence by BioMart were retained for the following analysis (minimum percentage identity > 80%). If a gene in the BMR could be aligned to multiple genes in the mouse genome, the gene with the highest sequence identity was kept for the following analysis. DESeq2 (ref. [67]) was used for differential expression analysis of orthologous genes between mouse and BMR. The main assumption in the library-size factor calculation of DESeq2 is that the majority of genes remain unchanged. To model the dispersion based on expression levels (mean counts of replicates), the dispersion for each gene is estimated using maximum-likelihood estimation. Considering the orthologs may have different gene lengths between species, gene lengths were considered by DESeq2 for read counts normalization between species. For the gene expression pattern of the *Dnmt1* gene in tissues, *Z*-scores were calculated for each tissue based on the normalized gene expression level of *Dnmt1*.

DNA methylation profiling array and MeDIP sequencing. Genomic DNA samples from young and dying BMR fibroblasts as well as mouse fibroblasts from low or high population doublings were extracted using a Zymo Quick-DNA miniprep plus kit. For the mammalian methylation array, DNA samples were sequenced using the custom Illumina chip 'HorvathMammalMethylChip40', which profiles about 37,000 CpGs that are highly conserved across mammals.

For MeDIP, genomic DNA was randomly sheared by sonication using a Covaris S2 instrument to a median fragment size of 200 bp. Using the NEBNext UltraII DNA library prep kit for Illumina (NEB), fragments were subjected to end repair with subsequent 3′ adenylation to create a 3′dA overhang suitable for adapter ligation. Adapter-ligated DNA was purified without size selection using Ampure XP beads. Methylated DNA was immunoprecipitated using a Zymo methylated-DNA IP kit and a 1:10 ratio of DNA to antibody. Library enrichment was performed using seven cycles of PCR. The resulting libraries were assessed for quantity and size. The amplified libraries were hybridized to the Illumina pair-end flow cell and amplified using the cBot (Illumina). Paired-end reads of 125 nucleotides were generated for each sample using a HiSeq 2500 sequencer (Illumina) at the University of Rochester Genomics Research Center. The MeDIP sequencing experiment was performed in two biological replicates.

The MeDIP sequencing reads were first trimmed using Trimmomatic[69] to remove adapter and other Illumina-specific sequences, together with low-quality bases, from the reads. The remaining high-quality reads, with a minimal length of 15 bp, were mapped to the BMR genome using STAR[64]. The entire genome was tiled into 100-bp windows and the aggregated methylation level for each sample in each window was then measured. As the chromosome information of the BMR genome is not available, only scaffolds with lengths > 10 kb were used. Differential methylation analysis was performed using edgeR, and genomic loci (that is, 100-bp windows) with an FDR < 0.1 were considered differentially methylated regions. Next, the adjacent differentially methylated windows were merged. Finally, the differentially methylated loci were functionally annotated according to their genomic loci (that is, overlap with genes or TEs).

Comet assay. DNA damage was detected using a commercial comet assay kit (Trevigen) following the manufacturer's guidelines. Basically, the cells were embedded in agarose, fixed and subjected to electrophoresis in a neutral buffer solution. The cells were stained with SYBR Gold and analyzed with microscopy. Images were acquired and the percentage of tail DNA was quantified from about 100 cells per sample using the CaspLab software.

DNA methylation and DNMT activity assay. Genomic DNA from BMR and mouse tissues or fibroblasts of different population doublings was purified using a Quick-DNA miniprep plus kit (Zymo). Purified genomic DNA (100 ng) was subjected to global DNA methylation measurement using an anti-5-methylcytosine (5-mC) antibody-based MethylFlash methylated DNA quantification kit (EpiGentek). For DNMT activities, nuclear proteins from human, mouse and BMR fibroblasts were extracted using an EpiQuik nuclear extraction kit (EpiGentek). Nuclear protein (1 μg) from each sample was subjected to DNMT activity measurement using an EpiQuik DNMT activity/inhibition assay ultra kit (EpiGentek).

NRTIs. The NRTIs (zidovudine (also known as azidothymidine, AZT) and abacavir (ABC)) used in this study were USP grade and obtained from Sigma.

Anchorage-independent soft-agar growth assay. One million exponentially growing fibroblasts from BMRs and mice were transfected by Amaxa with plasmids of the following combinations: 5 µg linearized pWZL-hygro-H-Ras V12, 5 µg pPB-LT (K1 or Δ434) and 5 µg pBase vectors. After transfection, the medium was changed and cells were selected with 2 µg ml^{-1} puromycin and 15 µg ml^{-1} hygromycin for 1 week to obtain integrated colonies. The colonies were pooled and infected with lentivirus-expressing sh-cGAS, sh-STING or sh-Scramble. For soft agar, 1% autoclaved Difco noble agar (BD Biosciences) was mixed with an equal volume of 2×MEM medium (Gibco) supplemented with 30% FBS and 2% penicillin–streptomycin. A 3 ml volume of mixture was poured into a 6 cm plate and allowed to solidify. The cells were harvested and counted. The cells (30,000) were mixed with 1.5 ml 2×complete MEM medium and then mixed with 1.5 ml of 0.8% autoclaved agar liquid, making a final 0.4% agar/1×media solution, poured on top of the solidified 0.5% medium agar and allowed to solidify at room temperature. The cells were cultured for 4 weeks. To visualize colonies, the plates were fixed with 70% cold ethanol for 1 h, washed three times with PBS, followed by the addition of 2 ml of 5 µg ml^{-1} ethidium bromide staining solution. After staining for 2 h, photos were taken under UV light using a Bio-Rad ChemiDoc imaging system. The experiments were repeated three times.

Tumor xenograft assay. The xenograft assay was performed as previously described[70]. Briefly, for each injection, 2×10^6 cells were collected and resuspended in 100 µl of ice-cold 50% Matrigel (BD Bioscience) in PBS. The mixed solution was subcutaneously injected into the flank in front of the hind legs of two-month-old female NIH III nude mice using a 22-gauge needle. The cells were allowed to grow for 8 weeks or until the size of the tumors reached 20 mm in the longest dimension before the mice were euthanized and the tumors were excised and analyzed. The size and weight of the tumors were recorded. If no signs of tumor growth were observed for 6 weeks, the mice were euthanized and dissected to verify the absence of tumors.

DMBA–TPA treatment. Three BMRs and three C57BL/6 mice were topically treated with DMBA and TPA. The BMRs and mice were topically treated with a single dose of DMBA (7.8 mM dissolved in acetone) on the dorsal trunk. After 3 d, treatment with 0.4 mM TPA three times a week was initiated. Two weeks after treatment, a skin biopsy was obtained from the treated area for RNA extraction and RT–qPCR. For tumorigenesis, hairless SKH1 mice were treated with the same initial dose of DMBA, followed by three TPA treatments per week for 12–15 weeks. For the treatments with demethylating agents, the mice were intraperitoneally injected with or without 0.5 mg kg^{-1} 5-Aza three times a week. For the NRTI treatment, the mice were provided with 1 mg ml^{-1} abacavir in their drinking water.

CCLE database analysis. RNA-seq data of 188 lung cancer cell lines were obtained from the Broad Institute (https://sites.broadinstitute.org/ccle/). Low-quality base calls and adapter sequences were trimmed using Trim_Galore. After trimming, reads longer than 50 bp were mapped to the GRCh37 build of the human genome reference by STAR[64] (GFF annotation of genes was from Gencode, release 34 and GFF annotation of repeat elements was from http://labshare.cshl.edu/ shares/mhammelllab/www-data/ TEtranscripts/TE_GTF/GRCh37_ GENCODE_rmsk_TE.gtf.gz). Alignments with less than 4% mismatch and at most 100 multiple alignments for a read were reported. Next, TEtranscripts[41] was used to measure the transcriptome abundance of TEs by combining transcripts of all instances of the same TE. Normalized read counts and expression levels were generated using DESeq2 (ref. [67]). Cell lines associated with mutations on genes of the type I IFN pathway (GOTERM_BP_ALL GO:0060337) were obtained from http://amp.pharm.mssm.edu/Harmonizome/. Mutations from the CCLE and COSMIC Cell Line Gene Mutation Profiles databases as well as the report of Klijn et al.[71] were collected. For outliers, the data was first sorted according to the 'number of mutations', the Z-scores were calculated for each data point based on the average and standard deviation for the whole number of mutations dataset, and cell lines with a Z-score > 3 or < -3 for the number of mutations were excluded as outliers. Next, the Z-scores for 'TE expression level' were calculated for each group of cell lines with the same number of mutations and cancer lines with a Z-score > 2 or < -2 for the TE expression level were excluded as outliers. The cell lines with the highest and lowest 25% of all TE expression were grouped and compared. Alternatively, the data were sorted by the sum of the LINEs expression and analyzed in the same method. Anandakrsihnan et al.[72] reported that three hits/mutations are required to develop lung adenocarcinoma; thus, cell lines with a mutation number ≥ 3 were separated from those with >2 mutations for comparison. Boxplots were generated. For the boxplots, the central rectangle ranges from the first quartile to the third quartile; the line in the rectangle shows the exclusive median and the whiskers indicate 1.5× the interquartile above the third quartile or 1.5× the interquartile below the first quartile. Outliers were not displayed in the boxplots but were included in the P-value calculation. $P < 0.05$ was considered as significant.

Reporting Summary. Further information on research design is available in the Nature Research Reporting Summary linked to this article.

Data availability

Most data are included in the figures. The exact P values, if applicable, are included in the source data. RNA-seq and MeDIP data have been deposited in the Gene Expression Omnibus (GEO) under accession no. GSE181413. Normalized methylation values of the Illumina microarray (HorvathMammalMethylChip40) are available at the GEO under accession no. GSE181732. The RNA-seq data of 188 lung cancer cell lines were obtained from the Broad Institute (https://sites.broadinstitute.org/ccle/). The cell-line mutation information was obtained from http://amp.pharm.mssm.edu/Harmonizome/. Source data are provided with this paper.

Code availability

All codes used in the current study have been deposited at https://github.com/qwzhang0601/ Transposon-triggered-innate-immune- response-confers-cancer-resistance- to-the-blind-mole-rat.

References

60. Birney, E., Clamp, M. & Durbin, R. GeneWise and Genomewise. *Genome Res.* **14**, 988–995 (2004).
61. Zhao, Y. et al. Naked mole rats can undergo developmental, oncogene-induced and DNA damage-induced cellular senescence. *Proc. Natl Acad. Sci. USA* **115**, 1801–1806 (2018).
62. Franken, N. A., Rodermond, H. M., Stap, J., Haveman, J. & van Bree, C. Clonogenic assay of cells in vitro. *Nat. Protoc.* **1**, 2315–2319 (2006).
63. Debacq-Chainiaux, F., Erusalimsky, J. D., Campisi, J. & Toussaint, O. Protocols to detect senescence-associated beta-galactosidase (SA-βgal) activity, a biomarker of senescent cells in culture and in vivo. *Nat. Protoc.* **4**, 1798–1806 (2009).
64. Dobin, A. et al. STAR: ultrafast universal RNA-seq aligner. *Bioinformatics* **29**, 15–21 (2013).
65. Tarailo-Graovac, M. & Chen, N. Using RepeatMasker to identify repetitive elements in genomic sequences. *Curr. Protoc. Bioinform.* **Chapter 4**, Unit 4.10 (2009).
66. Bao, W., Kojima, K. K. & Kohany, O. Repbase Update, a database of repetitive elements in eukaryotic genomes. *Mob. DNA* **6**, 11 (2015).
67. Love, M. I., Huber, W. & Anders, S. Moderated estimation of fold change and dispersion for RNA-seq data with DESeq2. *Genome Biol.* **15**, 550 (2014).
68. Yates, A. D. et al. Ensembl 2020. *Nucleic Acids Res.* **48**, D682–D688 (2020).
69. Bolger, A. M., Lohse, M. & Usadel, B. Trimmomatic: a flexible trimmer for Illumina sequence data. *Bioinformatics* **30**, 2114–2120 (2014).
70. Tian, X. et al. High-molecular-mass hyaluronan mediates the cancer resistance of the naked mole rat. *Nature* **499**, 346–349 (2013).
71. Klijn, C. et al. A comprehensive transcriptional portrait of human cancer cell lines. *Nat. Biotechnol.* **33**, 306–312 (2015).
72. Anandakrishnan, R., Varghese, R. T., Kinney, N. A. & Garner, H. R. Estimating the number of genetic mutations (hits) required for carcinogenesis based on the distribution of somatic mutations. *PLoS Comput. Biol.* **15**, e1006881 (2019).

Acknowledgements

This research was supported by grants from the US National Institutes of Health to Z. Zhang (grant no. AG047200), A.S. (grant no. AG047200) and V.G. (grant nos AG047200 and AG051449).

Author contributions

Y.Z., M.S., S.H., E.N., A.S. and V.G. designed the research. Y.Z. performed most of the experiments. E.O. performed the experiments with DNMT1 expression. J.L. performed the DNA-damage experiments. Q.Z., J.Y.L., Z. Zheng and Z. Zhang analyzed data. Z.K. and J.A. performed the DMBA–TPA experiments. Q.L., A.G., Y.S.L., J.H., J.L. and Z. Zheng provided help with experiments. A.S. and V.G. supervised the research. Y.Z., A.S. and V.G. wrote the paper with input from all authors.

Competing interests

The authors declare no competing interests.

Additional information

Extended data is available for this paper at https://doi.org/10.1038/s41590-021-01027-8.

Supplementary information The online version contains supplementary material available at https://doi.org/10.1038/s41590-021-01027-8.

Correspondence and requests for materials should be addressed to Andrei Seluanov or Vera Gorbunova.

Peer review information *Nature Immunology* thanks the anonymous reviewers for their contribution to the peer review of this work. Jamie D. K. Wilson was the primary editor on this article and managed its editorial process and peer review in collaboration with the rest of the editorial team.

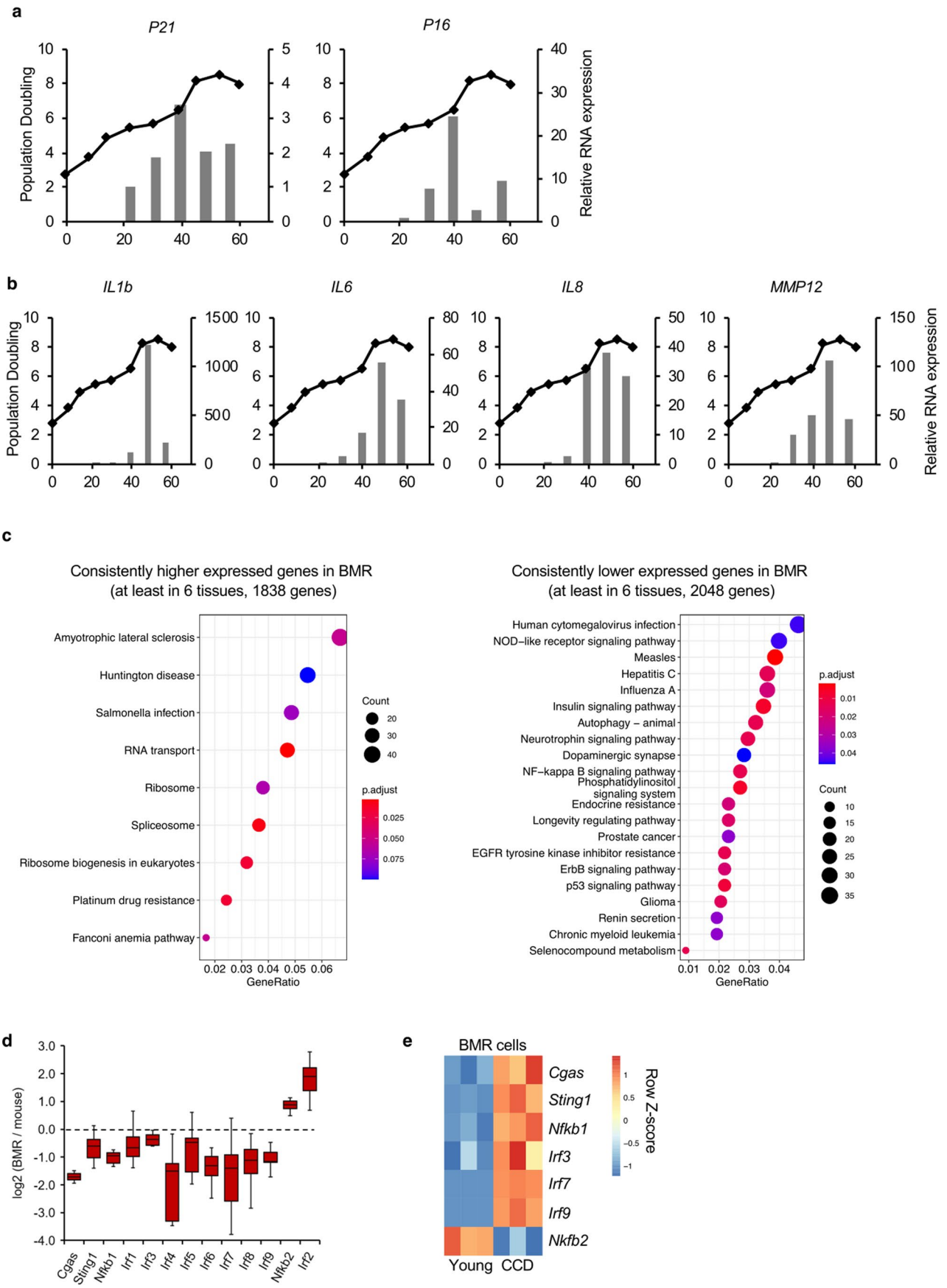

Extended Data Fig. 1 | See next page for caption.

Extended Data Fig. 1 | Activation of SASP in overproliferating BMR cells and differential gene expression in BMR and mice tissues. (**a**) qRT-PCR showing senescence markers *P21* and *P16* were increased with proliferation of BMR cells. (**b**) SASP factors *IL1b*, *IL6*, *IL8*, and *MMP12* were increased with proliferation of BMR cells. (**c**) KEGG pathway enrichment analysis of consistently upregulated and downregulated genes in the BMR tissues. RNA samples from 8 different tissues, including intestine, kidney, liver, lung, muscle, skin, spleen, and white adipose tissues (WAT) of BMR and mice were sequenced. A gene is defined as consistently upregulated gene if it expresses higher in BMR than in mice in at least six tissues. *P* values were adjusted by FDR. (**d**) A boxplot showing different fold changes of genes from IFN and NF-κB pathways comparing BMR and mice tissues. Center lines represent median, bounds of box are the 1st quartile and 3rd quartile, and whiskers are drawn down to the 10th percentile and up to the 90th percentile. (**e**) A heatmap showing differential gene expression in BMR CCD cells.

a

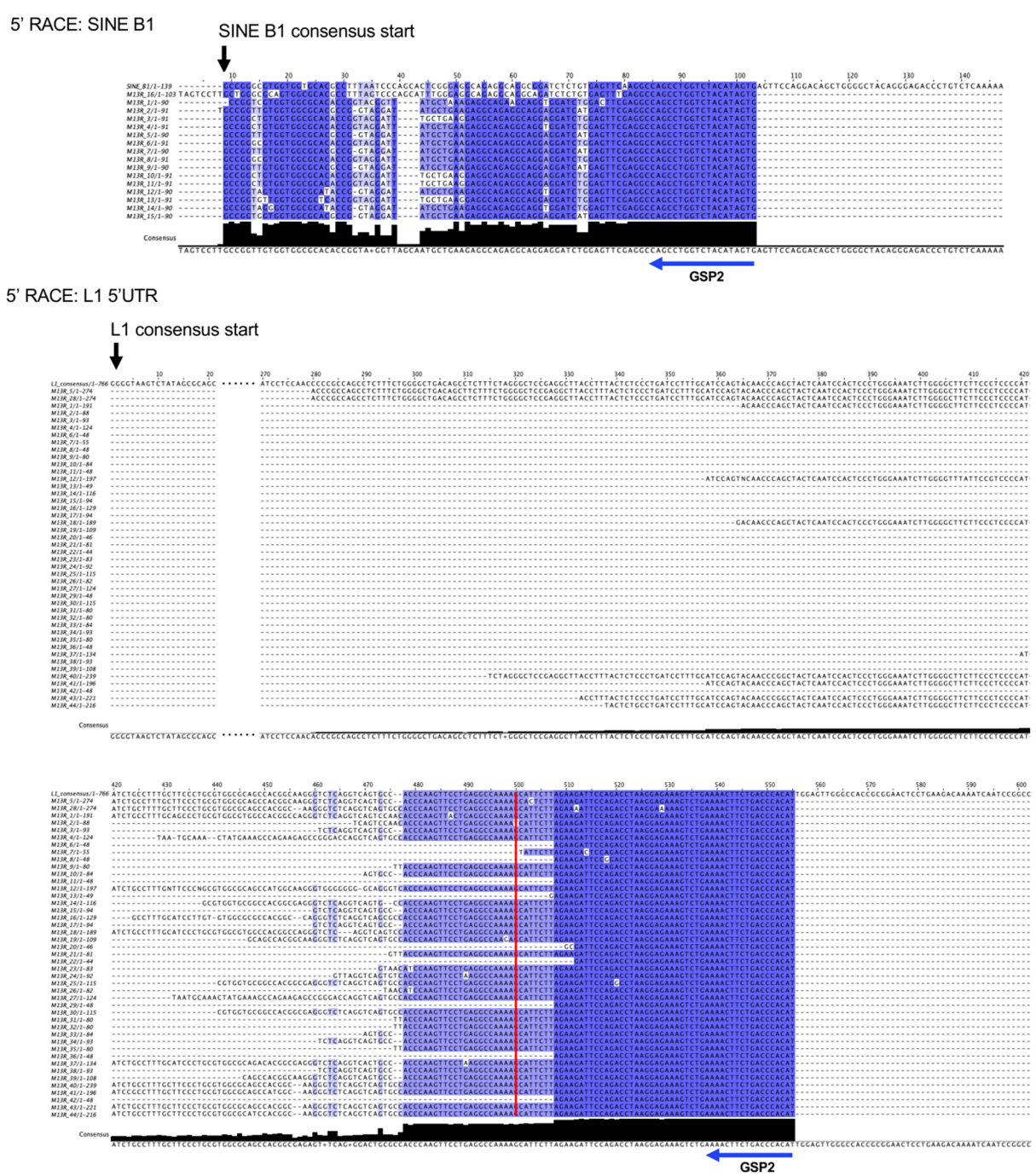

b

Summary of L1 5′ RACE

Sequenced clones	44
Start: < +180 bp	0
+180 bp to + 500 bp	34
> +500 bp	10

Extended Data Fig. 2 | Transcriptional start sites of B1 and L1 in BMR CCD cells. (**a**) Transcriptional start sites of B1 and L1 in CCD cells of BMR. 5′ RACE was performed using BMR fibroblasts undergoing CCD. The RACE product was ligated into T vector and colonies were sequenced. A multiple alignment of the products was generated against the consensus SINE B1 sequence or a predicted active L1 family homologous to mouse L1Mdal, respectively. The alignment was generated with Clustal Omega and displayed by Jalview. The location of gene-specific primer 2 (GSP2) for both B1 and L1 were shown under the consensus sequence. (**b**) Summary of the mapping data of L1 5′ RACE. The location of transcription start sites were shown relative to the consensus start site.

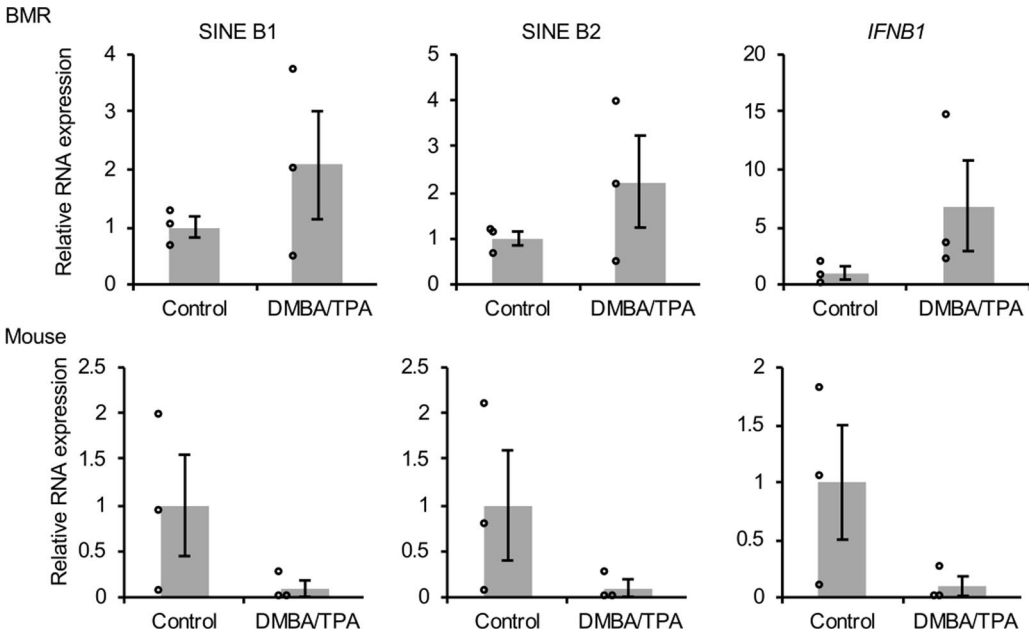

Extended Data Fig. 3 | RNA expression of SINE B1, B2 and *IFNB1* in carcinogen DMBA/TPA treated BMR and mouse skin. BMR and mice were topically treated with DMBA followed by treatment of TPA 3 days after DMBA. Two weeks after treatment, biopsy was taken from treated area, and RNA was extracted. Expression of SINE B1, B2 and IFNB1 was determined by qRT-PCR. Data are mean ± SEM of 3 biological replicates of 2 technical repeats.

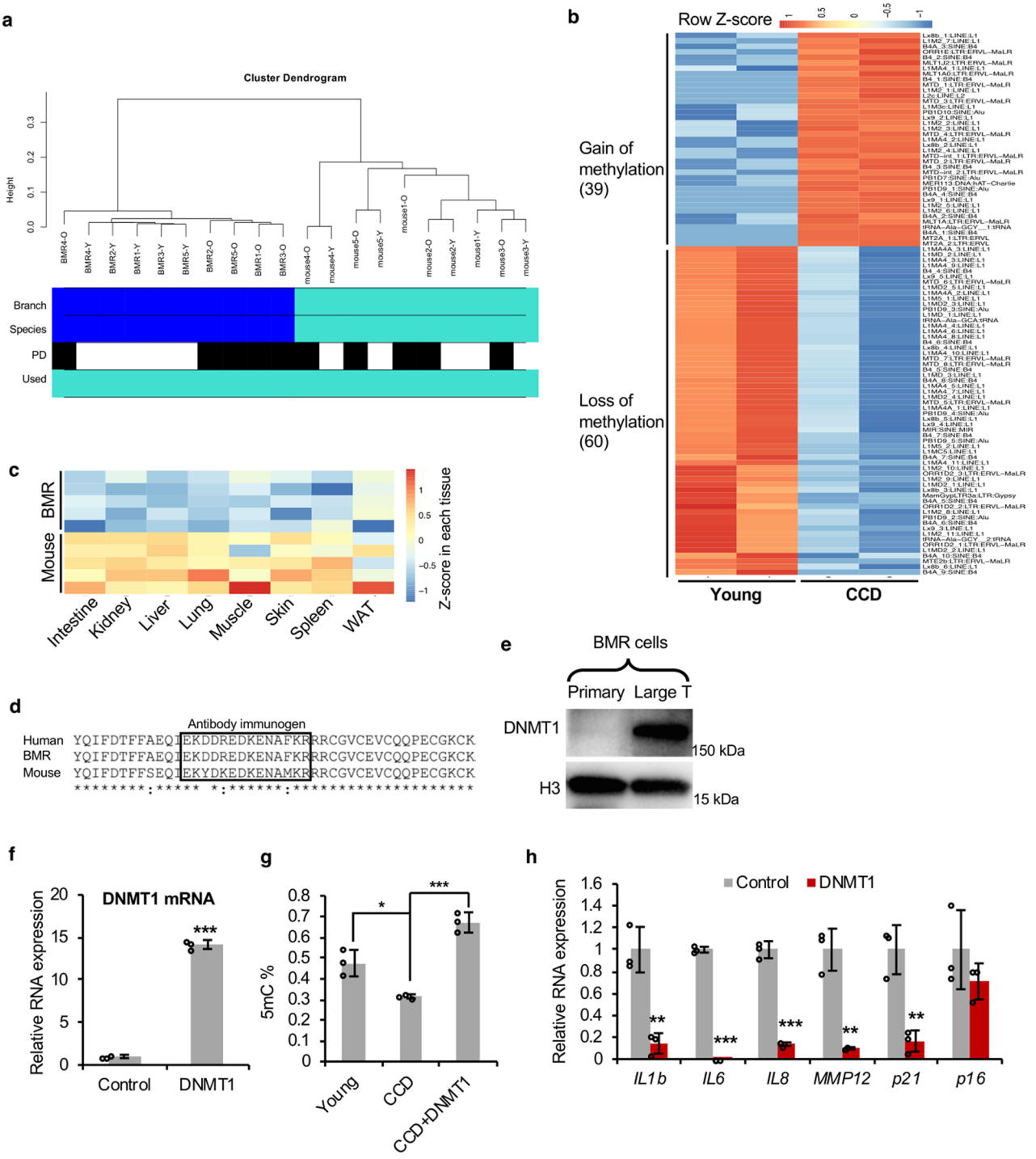

Extended Data Fig. 4 | Naturally low levels of DNMT1 result in loss of DNA methylation and SASP in overproliferating BMR cells. (**a**) Unsupervised hierarchical clustering of DNA samples from BMR and mouse fibroblasts with low and high PDs. The Average linkage hierarchical clustering is based on the inter-array correlation coefficient (Pearson correlation). The cluster branches (first color band) correspond to species (second color band, blue = BMR, cyan = mouse). Third color band: high PD (O; black) versus low PD (Y; white). (**b**) A heatmap showing differentially methylated elements determined using Methylated DNA immunoprecipitation (MeDIP). Differentially methylated regions (DMRs) were annotated against BMR genome. Totally 39 TE families were hyper-methylated and 60 TE families were hypo-methylated in dying BMR cells. Hypo-methylated TEs are enriched with B1 (especially PB1D9 family) and L1. (**c**) A heatmap showing generally lower expression levels of DNMT1 in 8 different tissues of BMR than mice. (**d**) alignment of partial sequence of human, mouse and BMR DNMT1 protein including immunogen recognized by the antibody used (Abcam ab13537). The immunogen is highly conserved across species, which is identical between human and BMR, and only 3 different amino acids different in mouse DNMT1. (**e**) Western blot detecting endogenous DNMT1 of primary and Large T transformed BMR cells. Large T is known to elevate DNMT1 expression. The significant band shows that the antibody is capable to detect BMR DNMT1. The experiment was repeated three times independently with similar results. (**f**) qRT-PCR showing overexpression of human DNMT1 in BMR cells. (**g**) Overexpression of DNMT1 restored global DNA methylation in BMR cells. (**h**) qRT-PCR showing repressed senescence factors by overexpression of DNMT1. Data are mean ± SD of 3 independent experiments. $^{*}P < 0.05$, $^{**}P < 0.01$, $^{***}P < 0.001$ by unpaired two-sided Student's t-test.

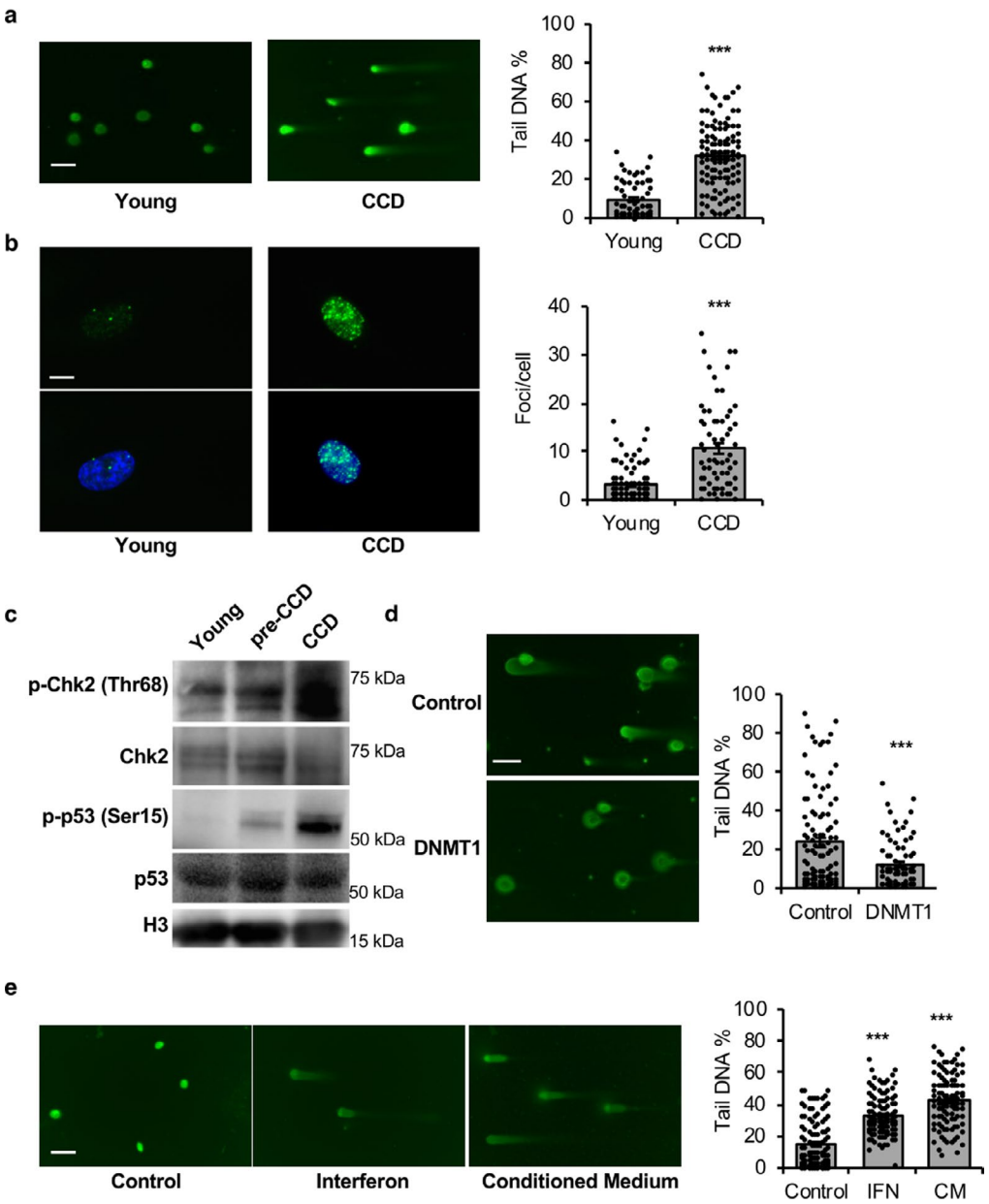

Extended Data Fig. 5 | BMR cells undergo DNA damage induced by IFN. (**a**) Images and quantification of comet assay detecting DNA damage of BMR cells with proliferation. Scale bar, 10 μM. (**b**) Images and quantification of immunofluorescence detecting γH2AX foci of BMR cells with proliferation. Scale bar, 5 μM. (**c**) DNA damage response of BMR cells with proliferation. Western blot was performed to show the phosphorylation of Chk2 (Thr68) and p53 (Ser15). The experiment was repeated three times independently with similar results. (**d**) Comet assay showing reduced DNA damage by overexpression of DNMT1. Scale bar, 10 μM. (**e**) Comet assay showing DNA damage induced by IFN. Young, growing BMR cells were treated with either medium containing BMR IFN or conditioned medium from old, dying BMR cells for 12 days before harvesting for comet assay. Scale bar, 10 μM. Tail DNA percentage (a, d, and e) or γH2AX (b) foci were quantified from 100 cells per group. Data are mean ± . $^{**}P < 0.01$, $^{***}P < 0.001$ by unpaired two-sided Student's t-test.

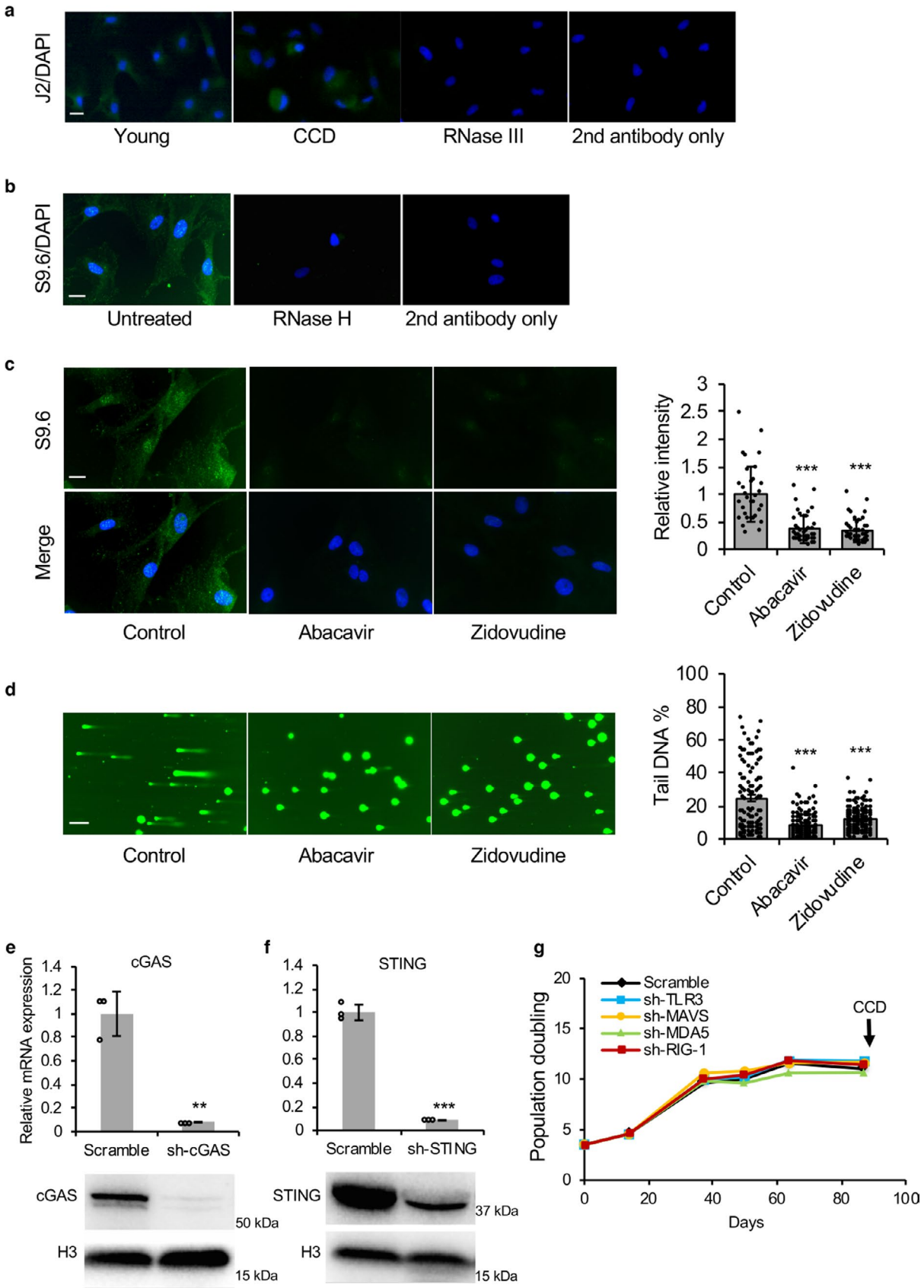

Extended Data Fig. 6 | See next page for caption.

Extended Data Fig. 6 | Nucleoside reverse-transcriptase inhibitors (NRTIs) treatment reduces RNA/DNA hybrids and represses cGAS–STING pathway. (**a**) Images of cytoplasmic double-stranded (ds) RNA in young and dying BMR cells stained with J2 antibody. Cells treated with RNase III and with secondary antibody only lost the signals, confirming the specificity of J2 antibody recognizing dsRNA. Scale bar, 5 μM. The experiment was repeated three times independently with similar results. (**b**) Images of cytoplasmic RNA/DNA hybrids in BMR cells stained with S9.6 antibody. Treatment of RNase H, which specifically degrades RNA/DNA hybrids, and with secondary antibody only didn't yield signals, confirming that S9.6 antibody specifically recognizes RNA/DNA hybrids. Scale bar, 5 μM. The experiment was repeated three times independently with similar results. (**c**) Reduced cytoplasmic RNA/DNA hybrids by NRTIs treatment stained by S9.6 antibody in BMR cells. Scale bar, 5 μM. Immunofluorescence intensities were quantified from 30 cells per group. (**d**) Comet assay showing reduced DNA damage by NRTIs treatment in BMR cells. Scale bar, 10 μM. Tail DNA percentages were quantified from 100 cells per group. (**e**-**f**) knockdown of cGAS (e) and STING (f) were determined by qRT-PCR and western blot. (**g**) growth curve showing that knockdown of dsRNA-sensing genes TLR3, MAVS, MDA-5, and IRG-1 didn't rescue CCD. Data are mean ± SD of 3 independent experiments. $^{**}P < 0.01$, $^{***}P < 0.001$ by unpaired two-sided Student's t-test.

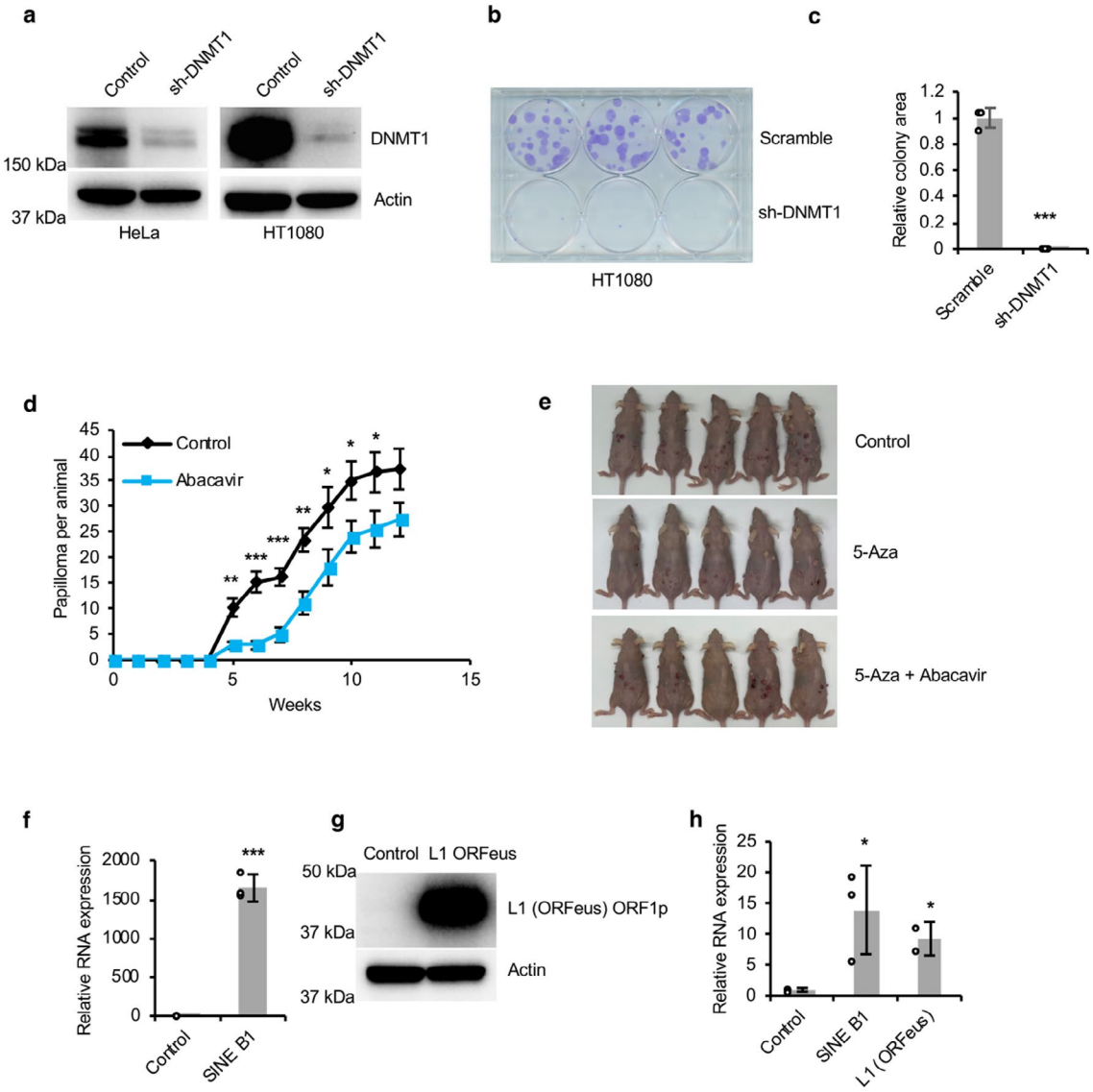

Extended Data Fig. 7 | Roles of DNMT1 and RTEs in tumorigenesis in mice and human cells. (**a**) Knockdown of DNMT1 in HeLa and HT1080 cancer cells as determined by Western blot. The experiment was repeated three times independently with similar results. (**b**-**c**) Knockdown of DNMT1 repressed proliferation of HT1080 cells in vitro. Clonogenic assay was performed with crystal violet staining and colonies areas were quantified (c). N = 3 technical replicates. Experiment was repeated three times independently with similar results. (**d**) Growth curve of DMBA/TPA-induced papilloma in mice treated with or without abacavir. Abacavir treated alone repressed DMBA/TPA induced papilloma. Experiment was performed using eight animals for each group. (**e**) Images of SKH1 hairless mice with papilloma induced by DMBA/TPA. 5-Aza repressed formation of papilloma, while abacavir restored this repression. (**f**) qRT-PCR showing overexpression of SINE B1 in HeLa cells. N = 3 technical replicates. (**g**) Western blot showing overexpression of L1 (ORFeus) in HeLa cells by detecting ORF1p. The experiment was repeated three times independently with similar results. (**h**) qRT-PCR showing activation of IFNB1 in HeLa cells by overexpression of SINE B1 and L1 (ORFeus). N = 3 technical replicates. Data are mean ± SD (c, f, and h) or mean ± SEM (d). * $P < 0.05$, ** $P < 0.01$, *** $P < 0.001$ by unpaired two-sided Student's t-test.

nature portfolio

Corresponding author(s): Vera Gorbunova
Andrei Seluanov

Last updated by author(s): Jul 27, 2021

Reporting Summary

Nature Portfolio wishes to improve the reproducibility of the work that we publish. This form provides structure for consistency and transparency in reporting. For further information on Nature Portfolio policies, see our Editorial Policies and the Editorial Policy Checklist.

Statistics

For all statistical analyses, confirm that the following items are present in the figure legend, table legend, main text, or Methods section.

n/a	Confirmed
☐	☒ The exact sample size (*n*) for each experimental group/condition, given as a discrete number and unit of measurement
☐	☒ A statement on whether measurements were taken from distinct samples or whether the same sample was measured repeatedly
☐	☒ The statistical test(s) used AND whether they are one- or two-sided *Only common tests should be described solely by name; describe more complex techniques in the Methods section.*
☒	☐ A description of all covariates tested
☒	☐ A description of any assumptions or corrections, such as tests of normality and adjustment for multiple comparisons
☐	☒ A full description of the statistical parameters including central tendency (e.g. means) or other basic estimates (e.g. regression coefficient) AND variation (e.g. standard deviation) or associated estimates of uncertainty (e.g. confidence intervals)
☐	☒ For null hypothesis testing, the test statistic (e.g. *F*, *t*, *r*) with confidence intervals, effect sizes, degrees of freedom and *P* value noted *Give P values as exact values whenever suitable.*
☒	☐ For Bayesian analysis, information on the choice of priors and Markov chain Monte Carlo settings
☒	☐ For hierarchical and complex designs, identification of the appropriate level for tests and full reporting of outcomes
☐	☒ Estimates of effect sizes (e.g. Cohen's *d*, Pearson's *r*), indicating how they were calculated

Our web collection on statistics for biologists contains articles on many of the points above.

Software and code

Policy information about availability of computer code

Data collection	Collection of qPCR data: ECFX Maestro™ Software by Bio-rad, version 1.0. Microscope imaging: NIS-Elements by Nikon, version 4.50. Immunoblot Imaging: ChemiDoc MP Imaging System by Bio-rad, version 3.0.1.
Data analysis	Excel was used to perform general statistical analyses (means, s.d., t-tests, etc). For RNAseq data analyses, the following software and codes were used: Trim_Galore (version 0.6.4), STAR (version 2.7.9a), RepeatMasker(version 4.07), TEtranscripts (version 2.2.1), DESeq2 (version 3.12), Ensembl BioMart (release 101). For MeDIP, the following softwares were used: EdgeR (version 3.1.3), Trimmomatic (version 0.39). For multiple alignment, the following softwares were used: Clustal Omega (release 1.2.2), Jalview (version 1.0). For L1 consensus prediction, the following software were used: GeneWise (version 2.2.0), ClustalW (version 2.1). ImageJ (version 1.50i) was used for immunofluorescence and western blot quantification. CaspLab (version 1.2.3beta2) was used for comet assay quantification.

For manuscripts utilizing custom algorithms or software that are central to the research but not yet described in published literature, software must be made available to editors and reviewers. We strongly encourage code deposition in a community repository (e.g. GitHub). See the Nature Portfolio guidelines for submitting code & software for further information.

Data

Policy information about availability of data

All manuscripts must include a data availability statement. This statement should provide the following information, where applicable:

- Accession codes, unique identifiers, or web links for publicly available datasets
- A description of any restrictions on data availability
- For clinical datasets or third party data, please ensure that the statement adheres to our policy

Most data are included in the figures. The exact p values, if applicable, are included in the source data. RNA-seq and MeDIP data have been deposited in the Gene Expression Omnibus (GEO) under accession no. GSE181413. Normalized methylation values of Illumina microarray (HorvathMammalMethylChip40) are available at GEO under accession no. GSE181732. RNA-seq data of 188 lung cancer cell lines were obtained from Broad Institute (https://sites.broadinstitute.org/ccle/). Cell line mutation information was obtained from http://amp.pharm.mssm.edu/Harmonizome/.

Field-specific reporting

Please select the one below that is the best fit for your research. If you are not sure, read the appropriate sections before making your selection.

☒ Life sciences ☐ Behavioural & social sciences ☐ Ecological, evolutionary & environmental sciences

For a reference copy of the document with all sections, see nature.com/documents/nr-reporting-summary-flat.pdf

Life sciences study design

All studies must disclose on these points even when the disclosure is negative.

Sample size	The size of all samples are described in figure legends for all experiments. Sample sizes were selected empirically from previous experimental experience with similar assays, and/or from sizes generally employed in the field. No statistical test was used to predetermine sample size.
Data exclusions	No exclusion of data was made.
Replication	All experimental data was reliably reproduced in multiple independent experiments as indicated in the figure legends.
Randomization	For in vivo tumor growth experiment, female NIH III nude mice aged 6 to 8 weeks were divided randomly into cages upon arrival and injected subcutaneously with 2×10e6 cells in Matrigel. No pre-established selection criteria for mice were used, other than gender and ages. When mice with desired gender were at appropriate ages, all mice in corresponding cages were used. No selection criteria were applied. Animals were assigned randomly by a technician that was blinded to the appearance or other characteristics of the animals.
Blinding	For all experiments, the investigators were blinded to group allocation during data collection. The investigators were blinded when quantifying immunofluorescence, soft agar, and comet assay results. Fields for quantification were randomly selected and scored, as indicated in Methods.

Reporting for specific materials, systems and methods

We require information from authors about some types of materials, experimental systems and methods used in many studies. Here, indicate whether each material, system or method listed is relevant to your study. If you are not sure if a list item applies to your research, read the appropriate section before selecting a response.

Materials & experimental systems

n/a	Involved in the study
☐	☒ Antibodies
☐	☒ Eukaryotic cell lines
☒	☐ Palaeontology and archaeology
☐	☒ Animals and other organisms
☒	☐ Human research participants
☒	☐ Clinical data
☒	☐ Dual use research of concern

Methods

n/a	Involved in the study
☒	☐ ChIP-seq
☒	☐ Flow cytometry
☒	☐ MRI-based neuroimaging

Antibodies

Antibodies used	The following antibodies were used: DNMT1 (Abcam ab13537; 1:1000), cGAS (Millipore ABF124; 1:1000 for western blot), STING (Thermo Fisher Scientific PA5-70420; 1:1000 for western blot), MX1 (Thermo Fisher Scientific PA5-22149; 1:1000 for western blot), p65 (Cell Signaling Technology 8242; 1:1000 for western blot), p-p65 S536 (Cell Signaling Technology 3033; 1:1000 for western blot), Chk2 (Cell Signaling Technology 2662; 1:1000 for western blot), p-Chk2 T68 (Cell Signaling Technology 2661; 1:1000 for western blot),

p53 (Cell Signaling Technology 2524: 1:500 for western blot), p-p53 S15 (Cell Signaling Technology 12571: 1:500 for western blot), S9.6 (Kerafast ENH001: 1:500 for immunofluorescence), J2 (Kerafast ES2001: 1:60 for immunofluorescence), LINE-1 ORF1p (Millipore MABC1152; 1:1000 for western blot), γH2AX (Millipore 05-636-I; 1:1000 for western blot), Horseradish peroxidase (HRP)-conjugated anti-rabbit IgG (Abcam ab6721; 1:5000 for WB), HRP-conjugated anti-mouse IgG (Abcam ab6789; 1:5000 for WB).

Validation

All antibodies are commercial and are listed in Methods section:

Immunoblot - DNMT1 - Abcam, ab13537
Species: Mouse, Rat, Human, Zebrafish
Application: IHC-P, IHC-Fr, ChIP, Flow Cyt, WB, IP

Immunoblot - cGAS - Millipore, ABF124
Species: Human, Mouse
Application: Western Blot, immunoprecipitation

Immunoblot - STING - Thermo Fisher Scientific, PA5-70420
Species: Bovine, Dog, Horse, Guinea pig, Human, Mouse, Pig, Rabbit, Rat
Application: Western Blot

Immunoblot - MX1 - Thermo Fisher Scientific, PA5-22149
Species: Human
Application: Immunohistochemistry, Western blot

Immunoblot - NF-kB p65 - Cell Signaling Technology, 8242
Species: Human, Mouse, Rat, Hamster, Monkey, Dog
Application: Western blot, Immunoprecipitation, Immunohistochemistry, Immunofluorescence , Flow cytometry, Chromatin Immunoprecipitation

Immunoblot - Phospho-NF-kB p65 (Ser536) - Cell Signaling Technology, 3033
Species: Human, Mouse, Rat, Monkey, Pig, Hamster
Application: Western blot, Immunoprecipitation, Immunofluorescence, Flow cytometry

Immunoblot - Chk2 - Cell Signaling Technology, 2662
Species: Human, Mouse, Rat, Monkey
Application: Western blog, Immunoprecipitation

Immunoblot - Phospho-Chk2 (Thr68) - Cell Signaling Technology, 2341
Species: Human, Monkey
Application: Western blog, Immunoprecipitation, Immunofluorescence, Flow cytometry

Immuoblot - p53 - Cell Signaling Technology, 2524
Species: Human, Mouse, Rat, Hamster, Monkey

Immunoblot - Phospho-p53 (Ser15) - Cell Signaling Technology, 12571
Species: Mouse, Rat
Application: Western blot, Immunoprecipitation

Immunoblot - Anti-LINE-1 ORF1p - Millipore, MABC1152
Species: Human
Application: Western blot, Immunocytochemistry, Immunoprecipitation, Immunohistochemistry

Immunofluorescence - S9.6 [DNA-RNA hybrid] - Kerafast, ENH001
Species: species independent
Application: Immunofluorescence

Immunofluorescence - J2 [dsRNA] - Kerafast, ES2001
Species: Mouse
Application: Immunofluorescence, Immunohistochemistry, ELISA, immuno-EM, Affinity purification

IImmunofluorescence - γH2AX - Millipore, 05-636-I
Species: Human, Mouse, Rat
Application: Western blot, Immunofluorescence, Immunocytochemistry, Immunoprecipitation

Immunoprecipitation - cGAS - Millipore, ABF124
Species: Human, Mouse
Application: Western Blot, Immunoprecipitation

Eukaryotic cell lines

Policy information about cell lines

Cell line source(s)

Primary fibroblasts were isolated from lung and skin of BMRs and mice of at least three individuals. Human primary skin fibroblasts HCA2 were obtained from Huffington Center on Aging and named by Olivia Pereira-Smith. 293T cells were only used for lentiviral packaging, and were obtained from Clontech. HeLa and HT1080 cells were obtained from ATCC.

Authentication	Fibroblast cell lines were authenticated using Short Tandem Repeat (STR) analysis as described in 2012 in ANSI Standard (ASN-0002) by the ATCC Standards Development Organization (SDO) and in Capes-Davis et al., Match criteria for human cell line authentication: Where do we draw the line? Int J Cancer. 2013;132(11):2510-9. 293T cell line was obtained from the sources above and used at low passage. They were not further authenticated. HeLa and HT1080 cells were obtained from ATCC and used at low passage. They were not further authenticated.
Mycoplasma contamination	All cells were mycoplasma-free with regular checks performed by a LookOut Mycoplasma PCR (i.e., polymerase chain reaction) Detection Kit (MP0035, Sigma-Aldrich).
Commonly misidentified lines (See ICLAC register)	None of these cell lines are listed in the International Cell Line Authentication Committee (ICLAC) database.

Animals and other organisms

Policy information about studies involving animals; ARRIVE guidelines recommended for reporting animal research

Laboratory animals	C57BL/6 mice of both sexes were purchased from Taconic Biosciences, Inc. Female NIH III Nude mice (Crl:NIH-Lystbg-JFoxn1nuBtkxid) and SKH1 hairless mice (Crl:SKH1-Hrhr) were purchased from Charles river Laboratories Inc. Mice were 6–12 weeks of age for all experiments, matched for age and sex, and kept under specific pathogen-free (SPF) conditions at the Animal center of University of Rochester. The mice were housed in 12-hour light/12-hour dark cycle, at temperature of 18-23 °C, with 40-60% humidity.
Wild animals	The blind mole rats (BMRs, Spalax galili) of both sexes were wild caught from Upper Eastern Galilee Mountains, Israel, by Biblical Zoo in Jerusalem, Israel, and transported to Rochester, NY by World Courier. As no exact age can be determined in wild animals, young adult BMRs were captured based on their body sizes (100-200g). BMRs were housed individually at room temperature with 24h dark cycle. Animals were euthanized by pentobarbital injection to collect tissues for RNA sequencing.
Field-collected samples	The study doesn't involve field-collected samples
Ethics oversight	All animal experiments were approved by University Committee on Animal Resources of University of Rochester.

Note that full information on the approval of the study protocol must also be provided in the manuscript.